American Mineralogist, Volume 78, pages 113–131, 1993

Octahedral excess mixing properties in biotite: A working model with applications to geobarometry and geothermometry

ALBERTO E. PATIÑO DOUCE
Department of Geology, University of Georgia, Athens, Georgia 30602, U.S.A.
A. DANA JOHNSTON, JACK M. RICE
Department of Geological Sciences, University of Oregon, Eugene, Oregon 97403, U.S.A.

ABSTRACT

Partial melting experiments on a natural metapelitic rock, reported by Patiño Douce and Johnston (1991), found the assemblage biotite + garnet + aluminosilicate + quartz + ilmenite (or rutile) over the P-T range 7–13 kbar, 825–975 °C. Compositions of coexisting biotite and garnet were used to investigate the nonideal solution behavior associated with mixing of Mg, Fe^{2+}, Al, and Ti in the octahedral layer in biotite. Our results show that contents of $^{[6]}Al$ and $^{[4]}Al$ in biotite are partially decoupled and that solution of $^{[6]}Al$ can be effectively modeled by means of dioctahedral exchange components of the form Al_2Mg_{-3} (Mg dioctahedral) and Al_2Fe_{-3} (Fe dioctahedral). Because these exchange components are equivalent to differences between additive components with known thermodynamic properties (muscovite-phlogopite and muscovite-annite, respectively) it is possible to use net-transfer equilibria between these exchange components and garnet, aluminosilicate, and quartz to estimate the absolute values of the interaction parameters W_{MgAl} and W_{FeAl} and of the differences $W_{AlTi} - W_{MgTi}$ and $W_{AlTi} - W_{FeTi}$. In order to account for the different octahedral site occupancies of phlogopite (or annite) and muscovite, we introduce an ideal mixing model for biotite that accounts for the nonequivalence of M1 and M2 octahedral sites in trioctahedral micas. Two sets of internally consistent interaction parameters were then derived by linear programming analysis, incorporating different assumptions about Fe^{3+} content in biotite in the experimental products. The values (in kJ/mol) for W_{MgAl}, W_{FeAl}, $W_{AlTi} - W_{MgTi}$ and $W_{AlTi} - W_{FeTi}$ are 52.2 or 54.7, 74.4 or 57.4, 47.8 or 65.1, and 60.1 or 75.1, respectively, with uncertainties on the order of 10 kJ/mol for W_{MgAl} and W_{FeAl} and 15 kJ/mol for $W_{AlTi} - W_{MgTi}$ and $W_{AlTi} - W_{FeTi}$. Equilibria involving dioctahedral exchange components in biotite allow us to carry out thermobarometric estimates in metapelitic rocks that are independent of plagioclase and of the (commonly low) grossular content of garnet. The biotite mixing model is applied in this way to generate internally consistent P-T estimates from natural biotite + garnet + aluminosilicate + quartz, biotite + cordierite + aluminosilicate + quartz, and biotite + garnet + cordierite + quartz assemblages, which agree with independent constraints on the values of these intensive variables. Such agreement indicates that the chemical potentials of the exchange components Al_2Mg_{-3} and Al_2Fe_{-3} and of their linear combination $MgFe_{-1}$ can be reliably estimated (at least within Al-rich bulk compositions) with the solution model that we propose.

INTRODUCTION

Trioctahedral micas are among the most abundant mafic minerals in the continental crust, where they play major roles in both igneous and metamorphic petrologic processes. The widespread distribution of biotite in pressure-temperature-composition space makes it a potentially fruitful source of information about the values of thermodynamic intensive variables under which such processes take place. Extraction of such information from mineral equilibria involving biotite, however, requires a sound understanding of the thermodynamic behavior of this complex solid solution as a function of temperature, pressure, and compositional variables. This same knowledge is necessary if we want to understand better petrologic processes, such as crustal anatexis or the formation of granulites, which in many crustal rocks are controlled to a large extent by terminal reactions of the micas.

In spite of the obvious importance of biotite as a rock-forming mineral, our knowledge of its solution properties is still rudimentary, in large part because the composition space of biotite is so extensive. The complexities of biotite solid solution are reflected in the fact that an adequate description of natural trioctahedral micas requires at least five or six linearly independent components (e.g., Dymek, 1983; Labotka, 1983; Guidotti, 1984; Hewitt and Abrecht,

0003–004X/93/0102–0113$02.00

1986). Compositions of natural trioctahedral micas show mixing of Mg, Fe^{2+}, Fe^{3+}, Al, Ti, and vacancies in octahedral sites, mixing of Si, Al, Fe^{3+} and, possibly, Ti in tetrahedral sites, mixing of K, Na, Ba, Ca, and vacancies in interlayer sites, and mixing of OH^-, O^{2-}, F^-, and Cl^- anions. Variable degrees of cation ordering, especially between divalent and tri- or tetravalent cations in the octahedral layer (e.g., Bailey, 1984; Brigatti et al., 1991), must also be considered when modeling the ideal mixing behavior of biotite. Even after such aspects of ideal mixing are accounted for, the excess energetic effects that arise from nonideal interactions among the different ions are likely to be important and must be determined and incorporated into solution models for trioctahedral micas.

In view of these difficulties, it is perhaps not surprising that utilization of mineral equilibria involving biotite in geothermometry and geobarometry is commonly problematic. A case in point is that of the geothermometer based on the Fe-Mg exchange equilibrium between biotite and garnet, which was calibrated experimentally by Ferry and Spear (1978) for biotite compositions along the phlogopite-annite join. It has become clear that temperatures calculated with this geothermometer using natural trioctahedral micas whose compositions depart from the phlogopite-annite join are often inaccurate and inconsistent with temperatures obtained from other mineral equilibria (e.g., Bohlen and Essene, 1980; Indares and Martignole, 1985; Edwards and Essene, 1987; Chipera and Perkins, 1988; Essene, 1989). Although the solution properties of garnet are also incompletely characterized, these inconsistencies appear to be particularly severe in upper amphibolite and granulite facies rocks, which recrystallized under pressure-temperature conditions at which biotite commonly incorporates important amounts of Ti, $^{[6]}$Al, vacancies, halogens, and oxy-components (e.g., Dymek, 1983; Guidotti, 1984).

A number of recent contributions have addressed the problem of estimating excess mixing properties in biotite and applying these mixing properties to improve the reliability of the garnet-biotite geothermometer. Indares and Martignole (1985) modeled the mixing of $^{[6]}$Al, $^{[6]}$Ti, $^{[6]}$Mg, and $^{[6]}$Fe in biotite with a regular solution model. They estimated the differences $W_{FeAl} - W_{MgAl}$ and $W_{FeTi} - W_{MgTi}$ from the compositions of natural garnet-biotite pairs, in which garnet cores were inferred to have equilibrated at a uniform temperature, during the peak of regional metamorphism, with matrix biotite isolated from garnet crystals. Hoisch (1989, 1991) also applied a regular solution model to the mixing of octahedral cations in biotite and estimated the values of the excess parameters W_{MgAl}, W_{FeAl}, and W_{TiAl} from the compositions of natural metamorphic biotites. The approach followed by Hoisch consisted of, in the first place, estimating equilibration temperatures from garnet-biotite Fe-Mg exchange equilibrium (either assuming ideal behavior, as did Ferry and Spear, 1978, or incorporating the excess parameters of Indares and Martignole, 1985) and estimating equilibration pressures from garnet + aluminosilicate + plagioclase + quartz equilibrium. These pressure-temperature conditions were then used to obtain biotite excess mixing parameters, utilizing the same biotite-garnet pairs from which pressures and temperatures were calculated by performing multiple linear regression on net-transfer equilibria involving the phlogopite, annite, eastonite, and siderophyllite components in biotite, the pyrope, almandine, and grossular components in garnet, and anorthite component in plagioclase. The circular nature of this approach calls into question the significance of the excess mixing parameters proposed by Hoisch (1991).

In another recent contribution, Williams and Grambling (1990) carried out a detailed statistical analysis of the effects of garnet and biotite compositions on the locus of the Fe-Mg exchange equilibrium between these two phases. They concluded that $^{[6]}$Al does not make a significant contribution to the nonideality of Fe-Mg mixing in biotite, or, in other words, that the difference between FeAl and MgAl interaction parameters is relatively small or negligible. In contrast, Williams and Grambling (1990) found that the effect of Ti on Fe-Mg mixing properties appears to be significant, but, because of multicolinearity in the data set used in their analysis, they could not obtain a reliable value for the contribution of Ti to the excess free energy of Mg-Fe mixing in biotite.

In this contribution we present experimental results that help to elucidate the compositional changes that take place in biotite in bulk compositions saturated with quartz, aluminosilicate, garnet, and titanium oxide phases, and we resolve some of the effects of these compositional changes on the excess Gibbs free energy of biotite. Our results confirm that Ti enrichment in biotite coexisting with Ti-saturating phases is a strong function of temperature. We also show that $^{[6]}$Al and $^{[4]}$Al are at least partially decoupled and that the content of $^{[6]}$Al in biotite coexisting with garnet, aluminosilicate, and quartz can be reliably modeled by means of net-transfer equilibria between these three phases and dioctahedral components in biotite. Linear programming analysis of the loci of these equilibria in pressure-temperature-composition space provides information about Mg-Fe-Al-Ti mixing properties in the dioctahedral layer of biotite, making it possible to estimate the absolute values of the interaction parameters W_{MgAl} and W_{FeAl} and the differences $W_{AlTi} - W_{MgTi}$ and $W_{AlTi} - W_{FeTi}$. We discuss applications of our results to thermometry and barometry of metapelitic rocks; in particular, we show how the $^{[6]}$Al content in biotite can be used as a reliable pressure indicator in assemblages that buffer the activity of alumina.

Experimental procedures

The results reported in this paper were derived from a series of dehydration-melting experiments on a natural metapelitic rock, originally designed to study the pressure, temperature, and compositional dependence of melt fraction during crustal anatexis (Patiño Douce and Johnston, 1991). For the bulk composition studied, we found

Table 1. Experimental conditions and phase assemblages

Exp.	*P* kbar	*T* °C	*t* h	Phase assemblage
APD-25	7	825	360	Qtz + Als + Bio + Gar + Ilm Melt
APD-22	7	850	336	Qtz + Als + Bio + Gar + Ilm Melt
APD-33	7	875	265	Qtz + Als + Bio + Gar + Ilm Melt
APD-34	7	900	118	Qtz + Als + Bio + Gar + Ilm Melt
APD-35	7	925	120	Qtz + Als + Bio + Gar + Ilm Melt
APD-43	7	950	77	Qtz + Als + Bio + Gar + Ilm + Rut Melt
APD-12	10	825	336	Qtz + Als + Bio + Gar + Ilm Melt
APD-11	10	850	336	Qtz + Als + Bio + Gar + Ilm Melt
APD-13	10	875	260	Qtz + Als + Bio + Gar + Ilm Melt
APD-4	10	900	120	Qtz + Als + Bio + Gar + Ilm + Rut Melt
APD-16	10	925	120	Qtz + Als + Bio + Gar + Rut Melt
APD-9	10	950	75	Qtz + Als + Bio + Gar + Rut Melt
APD-19	10	975	75	Qtz + Als + Bio + Gar + Rut Melt
APD-46	13	900	120	Qtz + Als + Bio + Gar + Rut Melt
APD-44	13	950	74	Qtz + Als + Bio + Gar + Rut Melt

that biotite persisted over a wide pressure-temperature range during progressive dehydration melting and that it changed very regularly in composition throughout that range. Because the pressure and temperature of each experiment are known and the grain size of the products is large enough to allow accurate electron probe analyses of all phases, it is possible to use these results to augment our understanding of the solution properties of biotite.

All experiments were performed under vapor-absent conditions and with a single starting material, a natural metapelitic rock (HQ-36) from northern Idaho (U.S.A.). The mineral assemblage of HQ-36 (biotite + muscovite + sillimanite + garnet + quartz + plagioclase + ilmenite) is described more fully in Patiño Douce and Johnston (1991, their Table 1), and it equilibrated at conditions approaching the second sillimanite isograd (Ruendal, 1987). Experiments were conducted at 7 and 10 kbar, at intervals of 25 °C above a minimum temperature of 825 °C, and at 13 kbar at 900 and 950 °C. Conditions and durations of the experiments, as well as phase assemblages of the experimental products, are given in Table 1. Note that the muscovite-out temperature has been exceeded in all experiments and that biotite is the only mica present in the products.

All the experiments reported in this paper were conducted in a piston-cylinder apparatus with NaCl-based cell assemblies 0.5 in. in diameter. The pressures reported are nominal pressures (Heise gauge) and are believed to be accurate to within 0.5 kbar (Bohlen, 1984). Experiments were pressurized at room temperature to 2 kbar below the target pressure and then heated to the target temperature, and then the pressure was adjusted to its nominal value. Because of thermal expansion, this final adjustment corresponded in every case to a pressure release (hot, piston out). Temperature was measured using $W_{74}Re_{26}$-$W_{95}Re_5$ thermocouples relative to an electronic ice point (0 °C) and controlled by a digital Eurotherm 808 temperature controller. Temperature stability throughout all experiments was better than ±5 °C. Samples were ground to less than 10 μm and contained in welded Au capsules. Utilization of small sample volumes (10–15 mg) resulted in the entire sample capsule being within 2–3 mm of the thermocouple. Further details about the experimental procedures can be found in Patiño Douce and Johnston (1991).

Controlling f_{O_2} in high-pressure experiments relies on the permeability of the capsule material to H_2 diffusion and on the presence of a vapor phase in the experimental charge that fixes the f_{H_2O}. Because no vapor phase was present in our experimental charges, control of f_{O_2} in them was not possible in practice. It has been found (e.g., Carroll and Wyllie, 1990) that the graphite furnace in the type of cell assembly used imposes redox conditions intermediate between the Ni + NiO and QFM buffers. The oxide mineral assemblage in the experimental products [ilmenite (Hm_{2-4}) ± rutile, see tables] and the garnet compositions (see below) are consistent with redox conditions of this order.

All successful experimental products were mounted in epoxy, sawed in half, and polished for electron beam analysis. Quantitative analyses were performed with a Cameca SX-50 microprobe utilizing a ZAF X-ray intensity reduction routine. Operating conditions were 15 kV, 20 nA, for garnet and ilmenite and 15 kV, 10 nA, for biotite, with a beam diameter of approximately 1 μm in every case. Between 15 and 25 different crystals of each phase (3–10 for the oxide phases) were analyzed in each experimental product. Mineral analyses are given in Tables 2, 3, and 4.

Because none of the experiments were reversed, the attainment of equilibrium cannot be rigorously demonstrated. The long durations of the experiments (especially at the lower temperatures investigated, see Table 1), and the presence of an H_2O-bearing melt which acted as a flux, facilitated reaction between solid phases. Additionally, a number of observations support an acceptable approach to equilibrium. Melt compositions and modes were found to change very regularly and consistently throughout the full pressure-temperature range investigated (Patiño Douce and Johnston, 1991), and the same is true of garnet, biotite, and ilmenite compositions (Tables 2, 3, and 4, respectively). Melt and mineral compositions (ex-

Table 2. Garnet compositions

P (kbar)	7	7	7	7	7	7	10	10
T (°C)	825	850	875	900	925	950	825	850
				Wt% oxides				
SiO_2	36.6	37.0	37.4	37.1	38.2	38.1	36.9	37.5
TiO_2	0.22	0.00	0.33	0.43	0.32	0.43	0.13	0.13
Al_2O_3	21.4	21.6	21.3	21.8	22.2	22.3	21.0	21.2
Cr_2O_3	0.00	0.04	0.00	0.02	0.06	0.00	0.02	0.00
MgO	5.05	5.35	6.75	7.64	10.0	11.0	5.01	5.13
CaO	1.19	0.98	0.59	0.53	0.26	0.39	1.28	1.46
MnO	1.20	1.18	0.44	0.36	0.13	0.31	1.26	1.11
FeO	32.1	32.2	31.8	30.1	27.7	25.5	32.4	32.9
Fe_2O_3	1.89	0.59	1.29	2.01	1.85	2.24	0.70	0.64
ZnO	0.08	0.08	0.00	0.02	0.04	0.07	0.03	0.00
TOTAL	99.8	99.1	99.8	100.1	100.7	100.3	98.7	100.1
				Cation contents				
Si	2.921	2.962	2.952	2.908	2.925	2.909	2.974	2.981
Ti	0.013	0.000	0.020	0.025	0.018	0.025	0.008	0.008
Al	2.017	2.037	1.980	2.015	2.003	2.004	1.992	1.984
Cr	0.000	0.000	0.000	0.001	0.004	0.000	0.001	0.000
Mg	0.601	0.638	0.795	0.891	1.141	1.250	0.602	0.607
Ca	0.102	0.084	0.050	0.044	0.021	0.032	0.111	0.124
Mn	0.081	0.080	0.030	0.024	0.008	0.020	0.086	0.075
Fe^{2+}	2.146	2.156	2.098	1.972	1.770	1.627	2.184	2.183
Fe^{3+}	0.113	0.036	0.077	0.118	0.106	0.129	0.042	0.038
Zn	0.005	0.005	0.000	0.001	0.002	0.004	0.000	0.000
Mg/Fe	0.280	0.296	0.379	0.452	0.645	0.768	0.276	0.278
Mg/Fe (min)	0.191	0.260	0.331	0.351	0.517	0.688	0.254	0.253
γ_{pyr}	1.322	1.275	1.181	1.141	1.065	1.057	1.346	1.352
γ_{alm}	1.001	1.010	1.026	1.035	1.065	1.065	1.000	0.996

Note: Values are single (rim composition) analyses from the crystal with highest Mg/Fe in each experiment (see text). Mg/Fe (min) is the minimum measured ratio for garnet rims in each experiment (see text). Typical uncertainties (counting statistics) are 1% (relative) for SiO_2 and FeO, 2% (relative) for Al_2O_3 and MgO, 8% (relative) for CaO and MnO. Stoichiometries calculated on the basis of eight cations and 12 O atoms; all residual negative charge assigned to Fe^{3+}. Fe_2O_3 wt% calculated from stoichiometry. Activity coefficients calculated with the model of Berman (1990), on a three-site basis.

cept garnet, discussed below) are also notably constant throughout any given charge. Linear programming analysis also shows that most of the experimental products (obtained over a temperature interval of more than 100 °C and with durations ranging from 3–15 d) are internally consistent. Most importantly, application of the biotite solution model derived from the experimental data to natural assemblages yields P-T estimates that agree with independent constraints for these intensive variables. We argue that all these observations taken as a whole cannot be easily dismissed as the product of coincidence in experiments that are far from equilibrium.

Mineral compositions

Garnet

Garnet produced by the dehydration-melting reaction of biotite nucleated on garnet initially present in the charges, but, because of slow cation diffusion rates, the crystals were not homogenized. Two clearly distinct compositional populations were therefore observed: cores corresponding to the initial, unreacted garnet and rims corresponding to garnet formed during the experiment. Because garnet grain size is typically small (about 10–15 μm) and the electron beam has a finite penetration (1–2 μm), the possibility exists that rim analyses included some core material from below the sample's surface. To minimize this effect, we chose as representative of each experiment the garnet rim analysis with the highest Mg/Fe ratio (i.e., with the Mg/Fe ratio most different from that of the unreacted cores). These Mg/Fe ratios (molar proportions) are listed in Table 2, together with the lowest measured Mg/Fe ratio for rim analyses in each experiment (included to illustrate the variability observed). The garnet present in the starting material has molar Mg/Fe = 0.188 (Patiño Douce and Johnston, 1991).

Garnet formulae were calculated from oxide percentages by assuming a total cation content of eight and a total anionic charge of 24. All residual negative charge was balanced with Fe^{3+}, resulting in calculated $Fe^{2+}/(Fe^{3+} + Fe^{2+})$ ratios varying between 0.94 and 0.99 (Table 2). Similar Fe^{3+}/Fe^{2+} ratios have been reported in electron probe analyses of garnet from natural high-grade metamorphic assemblages (e.g., Bohlen and Essene, 1980; Barbey et al., 1990; Sen Gupta et al., 1991). In order to ascertain whether the calculated Fe^{3+} values in the experimental products are reasonable, we used garnet compositions to estimate f_{O_2} in the experiments from the following net-transfer equilibrium (with standard-state thermodynamic properties from Berman, 1988, except for andradite, which was taken from Holland and Powell, 1990):

$$12(Fe^{3+}Al_{-1})_{gar} + 10Al_2SiO_5 + 2SiO_2 \leftrightarrow 4(Fe_3Al_2Si_3O_{12})_{gar} + 3O_2 \quad (1)$$

TABLE 2—*Continued*

P (kbar)	10	10	10	10	10	13	13
T (°C)	875	900	925	950	975	900	950
				Wt% oxides			
SiO_2	36.9	37.1	37.6	38.2	37.8	37.6	37.7
TiO_2	0.61	0.62	0.53	0.58	0.78	0.55	0.38
Al_2O_3	21.2	21.1	22.0	21.0	20.6	20.5	20.6
Cr_2O_3	0.00	0.04	0.05	0.04	0.03	0.05	0.00
MgO	6.43	6.99	7.98	9.70	9.69	7.79	8.46
CaO	0.76	0.87	0.45	0.32	0.42	0.56	0.54
MnO	0.49	0.77	0.17	0.17	0.18	0.20	0.33
FeO	31.7	30.5	30.5	28.4	27.9	30.6	29.2
Fe_2O_3	0.97	1.02	1.45	1.25	1.71	1.83	1.93
ZnO	0.07	0.00	0.00	0.03	0.00	0.07	0.10
TOTAL	99.1	99.0	100.8	99.7	99.0	99.8	99.2
				Cation contents			
Si	2.940	2.943	2.920	2.970	2.953	2.961	2.964
Ti	0.037	0.037	0.031	0.034	0.046	0.032	0.022
Al	1.988	1.976	2.011	1.917	1.900	1.902	1.914
Cr	0.000	0.003	0.003	0.003	0.002	0.003	0.000
Mg	0.764	0.828	0.923	1.122	1.130	0.913	0.992
Ca	0.065	0.074	0.037	0.026	0.035	0.047	0.046
Mn	0.033	0.052	0.011	0.011	0.012	0.013	0.022
Fe^{2+}	2.111	2.027	1.979	1.842	1.822	2.016	1.921
Fe^{3+}	0.058	0.061	0.084	0.073	0.101	0.108	0.114
Zn	0.004	0.000	0.000	0.002	0.000	0.004	0.006
Mg/Fe	0.362	0.408	0.466	0.609	0.620	0.453	0.516
Mg/Fe (min)	0.319	0.403	0.380	0.497	0.550	0.405	0.478
γ_{pyr}	1.215	1.198	1.139	1.077	1.071	1.153	1.124
γ_{alm}	1.021	1.028	1.052	1.061	1.088	1.039	1.061

where the exchange component $(Fe^{3+}Al_{-1})_{gar}$ is defined as

$$(Fe^{3+}Al_{-1})_{gar} = \tfrac{1}{2}(Ca_3Fe_2Si_3O_{12} - Ca_3Al_2Si_3O_{12}) \quad (2)$$

and its solution in garnet is assumed to be ideal. The results of this exercise are shown in Figure 1, together with f_{O_2} values along the QFM buffer equilibrium. Most experiments at 7 and 10 kbar yield f_{O_2} values about 2 log units above the QFM buffer, which are consistent with the redox conditions measured by Carroll and Wyllie (1990) in NaCl-graphite cell assemblies. This result creates confidence in the calculated Fe^{3+} values. Results from both experiments at 13 kbar suggest considerably more oxidized conditions (up to 4 log units above QFM). It is not clear whether this result reflects a change in the behavior of the cell assembly with pressure or whether it is a consequence of ignoring a possibly significant excess volume of mixing for the exchange component $(Fe^{3+}Al_{-1})_{gar}$.

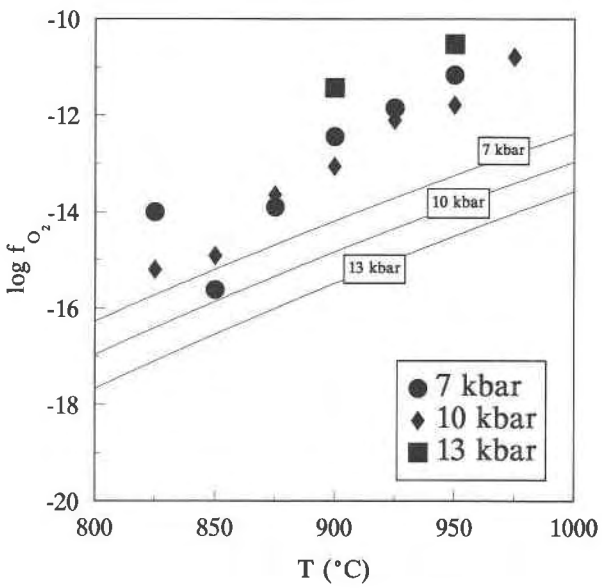

Fig. 1. The f_{O_2} values in experiments (symbols) estimated from garnet compositions (see text). For comparison, the curves show the loci of the QFM buffer at 7, 10, and 13 kbar (calculated with standard-state thermodynamic properties from Berman, 1988). Redox conditions somewhat more oxidizing than QFM are consistent with independent measurements of f_{O_2} in NaCl-graphite cell assemblies (Carroll and Wyllie, 1990).

Biotite

Biotite analyses were also complicated by grain size (5–10 μm), although in this case no compositional variation was detected within individual biotite crystals. The main issue was whether the biotite grain was too thin and some underlying glass was included in the analysis. Because the glass compositions are very silica-rich (about 70 wt% SiO_2, Patiño Douce and Johnston, 1991), this is detectable in the silica content of the biotite analysis, and all biotite analyses yielding more than 39 wt% SiO_2 were routinely discarded. All the remaining biotite analyses were averaged; these averages are listed in Table 3. The relative errors of these mean values (2 sd) are of essentially the

TABLE 3. Biotite compositions

P (kbar)	7	7	7	7	7	7	10	10
T (°C)	825	850	875	900	925	950	825	850
				Wt% oxides				
SiO_2	35.1	35.7	36.2	35.6	35.6	36.3	36.0	36.8
TiO_2	3.56	3.91	4.54	4.52	4.16	6.30	3.26	3.75
Al_2O_3	19.8	18.7	18.6	18.3	18.4	18.1	20.5	20.1
MgO	8.37	9.47	9.93	10.7	13.0	12.8	8.09	8.77
CaO	0.03	0.01	0.02	0.00	0.01	0.01	0.00	0.00
MnO	0.05	0.03	0.02	0.01	0.05	0.01	0.05	0.06
FeO*	19.1	18.3	17.5	16.5	13.3	13.2	19.0	18.0
Na_2O	0.23	0.16	0.15	0.17	0.53	0.21	0.18	0.17
K_2O	9.20	9.12	9.23	9.35	9.36	9.76	9.28	9.28
F	0.32	0.41	0.49	0.56	1.15	1.07	0.31	0.37
TOTAL	95.7	95.8	96.7	95.6	95.6	97.6	96.6	97.3
$Fe^{2+}/(Fe^{2+} + Fe^{3+})$	0.93	1.00	0.96	0.93	0.93	0.92	0.99	0.99
				Stoichiometries calculated including Fe^{3+}				
Si	2.656	2.690	2.693	2.673	2.661	2.646	2.686	2.718
$^{[4]}Al$	1.344	1.310	1.307	1.327	1.339	1.354	1.314	1.282
$^{[6]}Al$	0.417	0.352	0.325	0.296	0.282	0.199	0.492	0.463
Ti	0.202	0.222	0.254	0.256	0.234	0.346	0.183	0.208
Fe^{3+}	0.068	0.000	0.035	0.059	0.047	0.052	0.010	0.009
Mg	0.943	1.064	1.103	1.196	1.445	1.388	0.901	0.964
Fe^{2+}	1.122	1.153	1.048	0.963	0.775	0.740	1.172	1.096
Na	0.034	0.023	0.022	0.025	0.077	0.030	0.026	0.024
K	0.888	0.877	0.877	0.897	0.892	0.909	0.884	0.873
F	0.077	0.098	0.115	0.133	0.272	0.247	0.073	0.086
OH	1.923	1.902	1.885	1.867	1.728	1.753	1.927	1.914
TOTAL [4] + [6] cations	6.756	6.791	6.767	6.770	6.786	6.726	6.761	6.744
				Stoichiometries calculated assuming all Fe is Fe^{2+}				
Si	2.663	2.692	2.696	2.677	2.664	2.651	2.688	2.719
$^{[4]}Al$	1.337	1.308	1.304	1.323	1.336	1.349	1.312	1.281
$^{[6]}Al$	0.427	0.356	0.329	0.302	0.287	0.208	0.495	0.465
Ti	0.203	0.221	0.254	0.256	0.234	0.346	0.183	0.208
Mg	0.945	1.065	1.103	1.198	1.447	1.391	0.901	0.965
Fe^{2+}	1.209	1.153	1.093	1.037	0.834	0.807	1.184	1.108
Na	0.034	0.024	0.022	0.025	0.077	0.029	0.027	0.024
K	0.890	0.878	0.878	0.898	0.892	0.910	0.885	0.874
F	0.076	0.098	0.117	0.133	0.272	0.249	0.074	0.086
OH	1.924	1.902	1.883	1.866	1.728	1.751	1.925	1.913
TOTAL [4] + [6] cations	6.788	6.798	6.782	6.794	6.805	6.753	6.767	6.749

Note: Wt% values are means of 5–15 analyses of different crystals. Typical relative uncertainties of the mean values (2 sd) are 4% (relative) for SiO_2, K_2O and FeO*; 6% (relative) for Al_2O_3 and MgO; 15% (relative) for TiO_2 and F; 25% (relative) for Na_2O. FeO* = Total Fe as FeO. $Fe^{2+}/(Fe^{2+} + Fe^{3+})$ estimated from f_{H_2O} in melts and f_{O_2} from garnet compositions (see text). All stoichiometries calculated assuming total cation charge (except H) = +22.

same magnitude (4–6 relative %, see Table 3) for SiO_2, Al_2O_3, MgO, FeO, and K_2O in all the experimental products. Because the excitation volumes for these elements are not all the same, similarity in the relative errors of the means is a good indication that the values shown in Table 3 represent essentially uncontaminated biotite. Larger relative errors for TiO_2, F, and Na_2O are almost certainly derived from the poorer counting statistics for these elements, which are present in smaller concentrations.

Because all our analyses are electron beam analyses, the Fe^{3+} and H_2O contents of biotite were not determined. Furthermore, vacancies are known to occur in the structure of trioctahedral micas in high-grade metamorphic rocks (e.g., Holdaway, 1980; Guidotti, 1984). With these limitations, recalculation of a biotite analysis into a structural formula involves three unknown quantities, and a correct recalculation is impossible. Any recalculation scheme chosen must therefore entail some assumptions, which are discussed in the following paragraphs.

Hewitt and Wones (1984, p. 216–219), Partin (1984, in Hewitt and Wones, 1984), and Rebbert (1986) have discussed the effect of f_{H_2} on the Fe^{3+}/Fe^{2+} ratio of biotite. They suggested that, in Al-rich biotite (with more than about 10 mol% Tschermak's component), there are no major crystallographic constraints on the amount of Fe^{3+} and that Fe^{3+} content in such cases is primarily a function of the f_{H_2} under which the mica equilibrated. Because all our experimental biotites contain more than 10 mol% Tschermak's component, we argue that the last conclusion is also applicable to them. The Fe^{3+} content of biotite can then be roughly estimated from the f_{O_2} and f_{H_2O} in our experiments and the results of the authors cited above. In order to accomplish this, the f_{O_2} values calculated from Equilibrium 1 were used. The f_{H_2O} values were estimated from H_2O contents (calculated by mass balance) in the glasses coexisting with biotite (see Patiño Douce and Johnston, 1991), by means of the H_2O activity-composition model for silicate melts of Burnham (1979). The

TABLE 3—*Continued*

P (kbar)	10	10	10	10	10	13	13
T (°C)	875	900	925	950	975	900	950
				Wt% oxides			
SiO_2	36.4	36.4	36.1	36.6	37.9	37.0	37.1
TiO_2	4.51	4.59	5.08	5.74	5.38	4.94	5.85
Al_2O_3	19.9	19.6	19.8	19.1	19.5	20.1	18.8
MgO	9.31	10.4	10.2	11.2	13.4	9.43	9.93
CaO	0.01	0.01	0.01	0.00	0.00	0.00	0.02
MnO	0.02	0.02	0.02	0.03	0.01	0.01	0.01
FeO*	17.4	15.3	15.5	14.1	11.9	15.4	14.0
Na_2O	0.18	0.14	0.14	0.11	0.12	0.16	0.11
K_2O	9.40	9.36	9.39	9.49	9.79	9.54	9.60
F	0.41	0.58	0.53	0.88	1.29	0.44	0.63
TOTAL	97.5	96.4	96.8	97.3	99.2	97.0	96.1
$Fe^{2+}/(Fe^{2+} + Fe^{3+})$	0.97	0.96	0.95	0.96	0.94	0.95	0.94
				Stoichiometries calculated including Fe^{3+}			
Si	2.679	2.690	2.656	2.677	2.691	2.708	2.734
$^{[4]}Al$	1.321	1.310	1.344	1.323	1.309	1.292	1.266
$^{[6]}Al$	0.401	0.393	0.374	0.322	0.322	0.439	0.366
Ti	0.249	0.255	0.281	0.316	0.288	0.272	0.324
Fe^{3+}	0.026	0.031	0.039	0.028	0.034	0.038	0.042
Mg	1.021	1.143	1.119	1.225	1.419	1.028	1.090
Fe^{2+}	1.037	0.909	0.908	0.826	0.666	0.892	0.810
Na	0.026	0.020	0.020	0.016	0.017	0.023	0.016
K	0.882	0.882	0.882	0.885	0.888	0.890	0.902
F	0.095	0.136	0.123	0.203	0.290	0.102	0.147
OH	1.905	1.864	1.877	1.797	1.710	1.898	1.853
TOTAL [4] + [6] cations	6.735	6.731	6.722	6.718	6.730	6.670	6.632
				Stoichiometries calculated assuming all Fe is Fe^{2+}			
Si	2.682	2.693	2.661	2.679	2.694	2.711	2.738
$^{[4]}Al$	1.318	1.307	1.339	1.321	1.306	1.289	1.262
$^{[6]}Al$	0.406	0.397	0.382	0.325	0.328	0.445	0.373
Ti	0.249	0.255	0.282	0.316	0.288	0.272	0.324
Mg	1.022	1.145	1.121	1.226	1.421	1.029	1.091
Fe^{2+}	1.071	0.948	0.958	0.861	0.710	0.941	0.863
Na	0.025	0.020	0.020	0.016	0.016	0.023	0.017
K	0.884	0.883	0.883	0.886	0.889	0.891	0.903
F	0.096	0.135	0.123	0.204	0.291	0.102	0.147
OH	1.904	1.864	1.877	1.796	1.709	1.897	1.850
TOTAL [4] + [6] cations	6.750	6.747	6.744	6.730	6.747	6.688	6.652

TABLE 4. Ilmenite compositions

P (kbar)	7	7	7	7	7	7	10	10	10	10
T (°C)	825	850	875	900	925	950	825	850	875	900
					Wt% oxides					
SiO_2	0.11	0.11	0.09	0.09	0.19	0.11	0.09	0.04	0.08	0.21
TiO_2	52.4	50.8	51.2	51.1	51.6	51.6	51.0	51.2	50.2	50.6
Al_2O_3	0.19	0.26	0.30	0.40	0.36	0.45	0.21	0.23	0.25	0.47
Cr_2O_3	0.03	0.00	0.04	0.04	0.04	0.09	0.03	0.00	0.00	0.06
MgO	1.18	1.59	1.92	2.30	3.71	3.22	1.18	1.46	1.76	2.50
MnO	0.36	0.25	0.10	0.08	0.10	0.06	0.34	0.14	0.15	0.05
FeO	44.8	42.7	42.6	41.8	39.8	40.6	43.5	43.2	41.9	41.3
Fe_2O_3	0.76	2.09	2.10	2.14	1.59	1.50	2.43	2.15	2.84	2.69
ZnO	0.00	0.06	0.01	0.04	0.16	0.12	0.01	0.16	0.11	0.00
TOTAL	99.8	97.8	98.4	98.0	97.6	97.7	98.8	98.7	97.3	97.9
					Cation contents					
Si	0.003	0.003	0.002	0.002	0.005	0.003	0.002	0.001	0.002	0.005
Ti	0.987	0.973	0.973	0.971	0.974	0.975	0.971	0.975	0.967	0.961
Al	0.006	0.008	0.009	0.012	0.011	0.013	0.006	0.007	0.007	0.014
Cr	0.000	0.000	0.000	0.000	0.000	0.002	0.000	0.000	0.000	0.001
Mg	0.044	0.060	0.072	0.087	0.139	0.121	0.044	0.055	0.067	0.094
Mn	0.008	0.005	0.002	0.002	0.002	0.001	0.007	0.003	0.003	0.001
Fe^{2+}	0.938	0.909	0.900	0.884	0.835	0.854	0.922	0.915	0.896	0.871
Fe^{3+}	0.014	0.040	0.040	0.041	0.030	0.028	0.046	0.041	0.055	0.051
Zn	0.000	0.001	0.000	0.000	0.003	0.002	0.000	0.003	0.002	0.000

Note: Wt% values are means of at least three analyses of different crystals. Typical relative uncertainties of the mean values (2 sd) are 0.5% (relative) for FeO and TiO_2 and 8% (relative) for MgO and MnO. Stoichiometries calculated on the basis of two cations and three O atoms; all residual negative charge assigned to Fe^{3+}. Fe_2O_3 wt% calculated from stoichiometry.

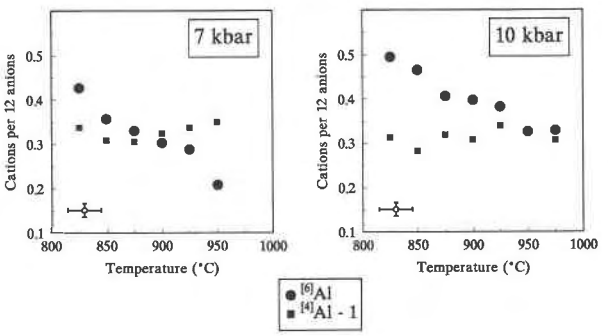

Fig. 2. Variations in [6]Al and excess [4]Al contents in experiments at 7 and 10 kbar (representative uncertainties shown by crosses). Decoupling between [4]Al and [6]Al is apparent.

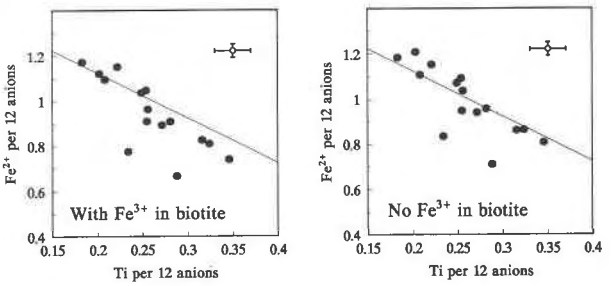

Fig. 3. Correlation between Fe^{2+} and Ti contents in experimental biotite (representative uncertainties shown by crosses). The lines correspond to the equation $Fe^{2+} = -2Ti$ + constant. The two points farther removed from the trend correspond to the experiments at 925 °C, 7 kbar and 975 °C, 10 kbar. The latter data point was rejected by all linear-programming optimization models.

values of f_{H_2}, calculated from f_{O_2}, f_{H_2O}, and the Gibbs free energy of formation of H_2O at the temperature of each experiment, were then used to estimate $Fe^{2+}/(Fe^{3+} + Fe^{2+})$ in biotite after Hewitt and Wones (1984, p. 218) and Rebbert (1986, p. 12–13). The resulting ratios, varying between 0.92 and 1.0, are shown in Table 3.

In order to test the effect of ignoring Fe^{3+} in modeling the solution properties of biotite and also because the procedure used to estimate Fe^{3+} is subject to large uncertainties, two sets of structural formulae for biotite are presented in Table 3. One set was calculated with the Fe^{3+} values discussed above, and the other set assuming that all Fe is Fe^{2+}. The relative merits of these two assumptions concerning Fe^{3+} content in biotite are discussed further in connection with the different sets of mixing parameters arising from them. Both sets of formulae in Table 3 were calculated on the basis of a total cationic charge in biotite (except H) of 22 (i.e., assuming that oxy-components are not present). Although the assumption of no oxy-components may not be entirely justified, given the high temperatures of the experiments, we believe that this is safer than assuming an arbitrary amount of oxy-components.

An examination of Table 3 reveals that biotite present in the experimental products departs from the ideal phlogopite-annite join in four important respects. These are the presence of excess [4]Al, the presence of [6]Al and [6]Ti, the substitution of F for OH, and the presence of vacancies in interlayer sites. It is important to examine in some detail the behavior of Al because equilibria involving Al-bearing exchange components in biotite are central to our discussion of excess mixing parameters in biotite. Figure 2 shows the variation in the contents of [6]Al and excess [4]Al (= [4]Al − 1) as a function of temperature for the experiments at 7 and 10 kbar. It is clear that, at least within the assemblage garnet + aluminosilicate + quartz + biotite, changes in the concentrations of [6]Al and [4]Al in biotite are not coupled. This observation implies that two linearly independent equilibria, involving at least two linearly independent components of biotite, are required to account for the total Al content of this phase. Previous workers (e.g., Robert, 1976; Dymek, 1983; Guidotti, 1984; Hewitt and Abrecht, 1986) have reached similar conclusions and have suggested that the two linearly independent Al-bearing exchange components that best describe biotite compositions are the Tschermak's component, $^{[6]}Al^{[4]}AlR_{-1}Si_{-1}$, and the dioctahedral component, $^{[6]}Al_2{}^{[6]}\square R_{-3}$ (where R stands for Mg or Fe, depending on whether phlogopite or annite, respectively, is chosen as the additive component of biotite). The total Al content in biotite present in the experimental products can then be modeled by means of the following three linearly independent net-transfer equilibria:

$$2Al_2SiO_5 + SiO_2 \leftrightarrow (Al_2Mg_{-3})_{bio} + (Mg_3Al_2Si_3O_{12})_{gar} \quad (3)$$

$$2Al_2SiO_5 + SiO_2 \leftrightarrow (Al_2Fe^{2+}_{-3})_{bio} + (Fe_3Al_2Si_3O_{12})_{gar} \quad (4)$$

$$\tfrac{4}{3}Al_2SiO_5 \leftrightarrow (Al_2Mg_{-1}Si_{-1})_{bio} + \tfrac{4}{3}SiO_2 + \tfrac{1}{3}(Mg_3Al_2Si_3O_{12})_{gar} \quad (5)$$

(note that the garnet-biotite Fe-Mg exchange is a linear combination of Eqs. 3 and 4).

Table 3 shows that the concentrations of Fe^{2+} and Ti in biotite vary antithetically with temperature. The correlation between both compositional variables, shown in Figure 3, has a slope close to −2, which is not significantly affected by whether Fe^{3+} is included in the biotite formulae. Such correlation is consistent with a Ti-vacancy exchange component of the form $^{[6]}Ti^{[6]}\square Fe^{2+}_{-2}$ (see also Holdaway et al., 1988). Although this particular exchange component is not the only possible way of interpreting Ti contents in biotite, Figure 3 does suggest that these contents can be modeled in pelitic compositions by equilibria such as

$$(TiFe^{2+}_{-2})_{bio} + (Fe_3Al_2Si_3O_{12})_{gar} \leftrightarrow (FeTiO_3)_{ilm} + Al_2SiO_5 + 2SiO_2 \quad (6)$$

or

$$3(TiFe^{2+}_{-2})_{bio} + 2(Fe_3Al_2Si_3O_{12})_{gar} \leftrightarrow 3TiO_2 + 2Al_2SiO_5 + 4SiO_2 \quad (7)$$

depending on whether ilmenite or rutile, respectively, is the Ti-saturating phase. We have found that the four exchange components Al_2Mg_{-3}, Al_2Fe_{-3}, $Al_2Mg_{-1}Si_{-1}$, and $TiFe_{-2}$ are sufficient to model the mixing behavior of Al-Ti-Mg-Fe components in biotite. Of course, a different set of four linearly independent exchange components could be equally satisfactory. Our particular choice of components is justified on the basis that it makes it possible to estimate excess mixing properties in biotite in a relatively straightforward fashion.

Ideal activity-composition relationships in aluminous and titaniferous biotite

Mixing of octahedral cations in biotite is commonly modeled as taking place on three indistinguishable sites. In order to evaluate whether this assumption is appropriate, it is necessary to discuss cationic ordering in biotite. The three octahedral sites in trioctahedral micas are not equivalent, the two M2 sites being smaller than the single M1 site (e.g., Bailey, 1984). This difference results in ordering of cations with different sizes in the structure of biotite. As discussed by Bailey (1984), ordering between Fe^{2+} and Mg is seldom observed in biotite, but ordering between these divalent cations and the smaller Al^{3+} cation is common in aluminous biotite, with Al^{3+} preferentially entering the M2 sites. It thus appears reasonable, at least as a first approximation, to model the octahedral layer in aluminous biotite by analogy with dioctahedral micas, in which $^{[6]}Al$ is restricted to the M2 sites and vacancies required by charge balance to the M1 site. Because Ti^{4+} and Fe^{3+} are closer in charge and size to Al^{3+} than to the divalent cations, it also appears reasonable to assume that these two cations are partitioned into the M2 sites. In the case of Ti^{4+}, further support for this hypothesis can be derived from the observation that incorporation of this cation is accompanied by the formation of vacancies (cf. Fig. 3; also Holdaway et al., 1988; Abrecht and Hewitt, 1988) and that these vacancies should preferentially form in the M1 site. It must be noted, however, that recent structural refinements of Ti-rich and Al-poor biotite from alkaline igneous rocks (Brigatti et al., 1991) do not support our model for Ti site occupancy, but it is not clear whether such results are applicable to biotite coexisting with Al-saturating phases. In any event, this discrepancy emphasizes the fact that caution must be exercised when applying the solution model proposed here beyond the composition space of aluminous metamorphic and igneous rocks, and it underscores the need for detailed structural studies of aluminous and titaniferous biotite.

If ordering between the two kinds of octahedral sites takes place in quaternary biotite solution (Mg-Fe^{2+}-$^{[6]}$Al-Ti), then the assumption that mixing of these cations occurs on three indistinguishable sites is not correct and should be abandoned. A better approach is to consider M2 and M1 as different crystallographic sites and to model mixing on each site independently. Additionally, because of the observed decoupling between the behaviors of $^{[6]}$Al and $^{[4]}$Al (cf. Fig. 2), mixing in the tetrahedral layer must also be considered independently and incorporated into the ideal activity-composition expression for each component of the solution.

Each exchange component is equivalent to the difference between two additive components. The two dioctahedral exchange components, which we will call Mg-dioctahedral (Mg-dic) and Fe-dioctahedral (Fe-dic), are defined by the differences (muscovite-phlogopite) and (muscovite-annite), respectively, whereas the Mg-Tschermak's exchange component (Mg-Tk) equals the difference: (eastonite-phlogopite). The chemical potentials, ideal activities, and activity coefficients of these exchange components are defined in terms of the corresponding variables for the additive components. Thus, for the Mg-dioctahedral exchange component:

$$\begin{aligned}\mu_{Mg\text{-}dic} &= \mu^0_{Mg\text{-}dic} + RT \ln a^{id}_{Mg\text{-}dic} + RT \ln \gamma_{Mg\text{-}dic} \\ &= \mu_{mus} - \mu_{phl} \\ &= \mu^0_{mus} - \mu^0_{phl} + RT \ln\left(\frac{a^{id}_{mus}}{a^{id}_{phl}}\right) + RT \ln\left(\frac{\gamma_{mus}}{\gamma_{phl}}\right) \end{aligned} \quad (8)$$

where:

$$\mu^0_{Mg\text{-}dic} = \mu^0_{mus} - \mu^0_{phl} \quad (9)$$

and

$$a^{id}_{Mg\text{-}dic} = \frac{a^{id}_{mus}}{a^{id}_{phl}}. \quad (10)$$

Similarly,

$$a^{id}_{Fe\text{-}dic} = \frac{a^{id}_{mus}}{a^{id}_{ann}} \quad (11)$$

and

$$a^{id}_{Mg\text{-}Tk} = \frac{a^{id}_{eas}}{a^{id}_{phl}}. \quad (12)$$

These relationships show that, in order to calculate the ideal activities of the exchange components chosen to describe biotite composition, it is necessary to determine expressions for the ideal activities of phlogopite, annite, muscovite, and eastonite in a trioctahedral mica. A rigorous application of the method of Kerrick and Darken (1975), with the cationic ordering assumptions discussed above, leads to the following expressions for the contributions of tetrahedral, M1, and M2 sites to the ideal activities of phlogopite, muscovite, and eastonite in biotite solid solution (mole fractions are defined in Table 5).

Contributions from the tetrahedral site are calculated by considering mixing of Si and Al on four indistinguishable sites. The resulting tetrahedral contributions to the ideal activities of muscovite, phlogopite, and eastonite

TABLE 5. Mole fractions for activity-composition expressions

Tetrahedral sites

$$X_{Si} = \frac{Si}{4}$$

$$X_{^{[4]}Al} = \frac{^{[4]}Al}{4}$$

Octahedral M1 site

$$X_{^{M1}Mg} = \frac{Mg}{Mg + Fe^{2+}} \cdot (\Sigma - 6)$$

$$X_{^{M1}Fe} = \frac{Fe^{2+}}{Mg + Fe^{2+}} \cdot (\Sigma - 6)$$

$$X_{\square} = 7 - \Sigma$$

Octahedral M2 sites

$$X_{^{M2}Mg} = \frac{Mg}{Mg + Fe^{2+}} \cdot \frac{2 - {}^{[6]}Al - Ti - Fe^{3+}}{2}$$

$$X_{^{M2}Fe} = \frac{Fe^{2+}}{Mg + Fe^{2+}} \cdot \frac{2 - {}^{[6]}Al - Ti - Fe^{3+}}{2}$$

$$X_{^{M2}Al} = \frac{^{[6]}Al}{2}$$

$$X_{^{M2}Ti} = \frac{Ti}{2}$$

Note: Biotite stoichiometry on 12-anion basis; Σ = total sum of octahedral plus tetrahedral cations.

($a^{id,tet}$) are

$$a^{id,tet}_{mus} = a^{id,tet}_{phl} = \frac{256}{27} X_{^{[4]}Al} X^3_{Si}$$

$$a^{id,tet}_{eas} = 16 X^2_{^{[4]}Al} X^2_{Si}. \quad (13)$$

This model for tetrahedral mixing is consistent with the suggestion of Bailey (1984) that Si-Al ordering in the tetrahedral layer of micas is not common, although recent spectroscopic studies (Circone et al., 1991) indicate that long-range Al-Si ordering may be the norm in Al-rich biotite. Tetrahedral contributions enter the activity-composition expression of the Mg-Tk exchange component, but they cancel out in those of the dioctahedral exchange components, which are the ones utilized in our determination of excess mixing properties. Elimination of tetrahedral contributions in the ideal activities of the dioctahedral exchange components, however, is not strictly justified if Si-Al ordering differs in end-member muscovite, phlogopite, and annite. In other words, the preliminary solution model developed here ignores possible energetic effects arising from different degrees of Al-Si ordering that could be coupled to the total Al content of biotite. Detailed experimental studies and structural refinements are required to clarify this problem.

Following our assumptions about octahedral ordering in biotite, the contribution of M1 octahedral cations is calculated by considering mixing of Mg, Fe^{2+}, and vacancies on a single site:

$$a^{id,M1}_{eas} = a^{id,M1}_{phl} = X_{^{M1}Mg}$$

$$a^{id,M1}_{mus} = X_{\square}. \quad (14)$$

Finally, mixing of Mg, Fe^{2+}, Fe^{3+}, Al, and Ti on two indistinguishable M2 octahedral sites leads to

$$a^{id,M2}_{phl} = X^2_{^{M2}Mg}$$

$$a^{id,M2}_{mus} = X^2_{^{M2}Al}$$

$$a^{id,M2}_{eas} = 4 X_{^{M2}Mg} X_{^{M2}Al}. \quad (15)$$

Because it is also assumed that no Fe^{2+}-Mg ordering takes place, the Mg/Fe^{2+} ratio in M1 and M2 sites is the same. This premise is incorporated in the expressions for the mole fractions of Mg and Fe^{2+} shown in Table 5.

The ideal activity of each of the additive components phlogopite, muscovite, and eastonite is the product of the three corresponding partial contributions listed above, together with the contributions from anions and interlayer cations, resulting in

$$a^{id}_{phl} = \frac{256}{27} X^2_{^{M2}Mg} X_{^{M1}Mg} X_{^{[4]}Al} X^3_{Si} X_K X^2_{OH^-}$$

$$a^{id}_{mus} = \frac{256}{27} X^2_{^{M2}Al} X_{\square} X_{^{[4]}Al} X^3_{Si} X_K X^2_{OH^-}$$

$$a^{id}_{eas} = 64 X_{^{M2}Mg} X_{^{M2}Al} X_{^{M1}Mg} X^2_{^{[4]}Al} X^2_{Si} X_K X^2_{OH^-}. \quad (16)$$

An expression entirely analogous to that for phlogopite can be written for annite by replacing all Mg mole fractions with the corresponding Fe^{2+} mole fractions from Table 5. Note that the phlogopite and annite activity-composition relationships collapse to the familiar activity expressions if biotite composition is restricted to the pure trioctahedral annite-phlogopite join. For example, in the case of phlogopite, $^{[6]}Al = Ti = Fe^{3+} = 0$; $^{[4]}Al = K = 1$; $Si = 3$; $OH^- = 2$, and the activity expression becomes

$$a^{id}_{phl} = \left(\frac{Mg}{Mg + Fe}\right)^3 \quad (17)$$

as expected.

The ideal activities of the Mg-dioctahedral ($a_{Mg\text{-}dic}$) and Fe-dioctahedral ($a_{Fe\text{-}dic}$) exchange components are given by

$$a^{id}_{Mg\text{-}dic} = \frac{a^{id}_{mus}}{a^{id}_{phl}} = \frac{X^2_{^{M2}Al} X_{\square}}{X^2_{^{M2}Mg} X_{^{M1}Mg}} \quad (18)$$

$$a^{id}_{Fe\text{-}dic} = \frac{a^{id}_{mus}}{a^{id}_{ann}} = \frac{X^2_{^{M2}Al} X_{\square}}{X^2_{^{M2}Fe^{3+}} X_{^{M1}Fe^{2+}}} \quad (19)$$

in which all tetrahedral contributions cancel out. The ideal activity of the Mg-Tschermak's component ($a^{id}_{Mg\text{-}Tk}$) simplifies to

$$a^{id}_{Mg\text{-}Tk} = \frac{a^{id}_{eas}}{a^{id}_{phl}} = \frac{27 X_{^{M2}Al} X_{^{[4]}Al}}{4 X_{^{M2}Mg} X_{Si}} \quad (20)$$

which preserves the contribution of tetrahedral Al-Si mixing (compare Hoisch, 1991).

Nonideal mixing behavior of aluminous and titaniferous biotite

Calculated values of the ideal activities of the dioctahedral exchange components ($a^{id}_{Mg\text{-}dic}$ and $a^{id}_{Fe\text{-}dic}$) in biotite present in the experimental products are shown in Figure 4 (for biotite stoichiometry calculated assuming that Fe^{3+} is present, see Table 3). These ideal activities vary in regular and consistent ways with pressure and temperature (with the possible exception of the experiment at 975 °C, 10 kbar), and this behavior is not affected if Fe^{3+} in biotite is neglected (not shown in Fig. 4). Such regular trends support the choice of the Mg-dioctahedral and Fe-dioctahedral exchange components to model the $^{[6]}Al$ content in biotite. The importance of this result resides in the fact that Reactions 3 and 4 can also be written in terms of additive components whose thermodynamic properties are known, as follows:

$$KMg_3AlSi_3O_{10}(OH)_2 + 2Al_2SiO_5 + SiO_2 \leftrightarrow KAl_2AlSi_3O_{10}(OH)_2 + Mg_3Al_2Si_3O_{12} \quad (21)$$

$$KFe_3AlSi_3O_{10}(OH)_2 + 2Al_2SiO_5 + SiO_2 \leftrightarrow KAl_2AlSi_3O_{10}(OH)_2 + Fe_3Al_2Si_3O_{12}. \quad (22)$$

The Gibbs free energy changes of Reactions 21 and 22 can be calculated at any given pressure and temperature, and from these free energy changes it is possible, by comparing Reactions 21 and 22 with Reactions 3 and 4, respectively, to derive the chemical potentials of the Mg-dioctahedral and Fe-dioctahedral exchange components in biotite. Although other choices of exchange components could describe biotite composition as well as the dioctahedral components, no other choice leads to an equally reliable way of determining the actual values of the chemical potentials of the exchange components.

Assuming that quartz and aluminosilicate are pure phases, the equilibrium constants for Reactions 3 and 4 can be written as follows:

$$K_3 = a^{id}_{Mg\text{-}dic}\gamma_{Mg\text{-}dic}(X^{gar}_{Mg})^3\gamma_{pyr} \quad (23)$$

$$K_4 = a^{id}_{Fe\text{-}dic}\gamma_{Fe\text{-}dic}(X^{gar}_{Fe})^3\gamma_{alm}. \quad (24)$$

The excess chemical potentials of the Mg-dioctahedral and Fe-dioctahedral exchange components in biotite solid solution are then given by (respectively)

$$\mu^{ex}_{Mg\text{-}dic} = RT \ln \gamma_{Mg\text{-}dic} = RT(\ln K_3 - \ln K_3^*) \quad (25)$$

and

$$\mu^{ex}_{Fe\text{-}dic} = RT \ln \gamma_{Fe\text{-}dic} = RT(\ln K_4 - \ln K_4^*) \quad (26)$$

where

$$\ln K_3^* = \ln[a^{id}_{Mg\text{-}dic}(X^{gar}_{Mg})^3\gamma_{pyr}] \quad (27)$$

and

$$\ln K_4^* = \ln[a^{id}_{Fe\text{-}dic}(X^{gar}_{Fe})^3\gamma_{alm}]. \quad (28)$$

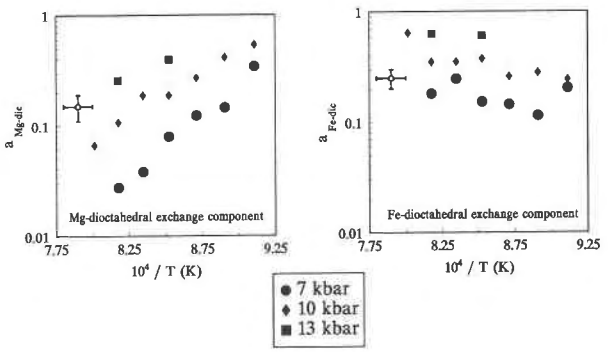

Fig. 4. Ideal activities of Mg-dioctahedral exchange component (Eq. 18) and Fe-dioctahedral exchange component (Eq. 19), for biotite stoichiometries calculated with Fe^{3+}. Representative uncertainties (shown by crosses) estimated by propagating uncertainties in biotite compositions (see text). Note that, because of logarithmic and inverse scales, graphical size of error bars changes with coordinate values.

Values of $\ln K_3^*$ and $\ln K_4^*$, calculated from biotite and garnet compositions in the experimental products, are shown in Table 6. These values include nonideality in garnet calculated with the solution model of Berman (1990). The values of γ_{pyr} and γ_{alm} calculated with this model (on a three-site basis, rather than the one-site basis presented by Berman) are shown in Table 2. Note that the activity coefficients for pyrope and almandine are close to 1, reflecting the low Ca and Mn contents in the garnets that grew during the experiments. Also shown in Table 6 are the values of $\ln K_3$ and $\ln K_4$, calculated from the equilibria among pure end-member additive components (Reactions 21 and 22, respectively) with standard-state thermodynamic properties from Berman (1988, 1990). The aluminosilicate polymorph used in calculating these equilibrium constants was sillimanite at 7 and 10 kbar and kyanite at 13 kbar, and β-quartz was assumed to be the stable SiO_2 polymorph in all the experiments.

Departure of the equilibrium positions from those predicted by ideal behavior of biotite can be appreciated in Figure 5 (for biotite stoichiometry, assuming that Fe^{3+} is present), as a function of pressure and of the inverse of temperature. These diagrams show that solution of $^{[6]}Al$ in magnesium iron aluminum titanium biotite is far from ideal. The excess chemical potentials of the dioctahedral exchange components are in the range 30–45 kJ/mol (see Table 6). For comparison, the standard-state molar Gibbs free energy of the Mg-dioctahedral exchange component, defined as the difference between the standard-state molar Gibbs free energies of muscovite and phlogopite, is on the order of 280 kJ/mol (at 10 kbar, 800 °C). The excess chemical potentials are clearly not negligible. Note from Figure 5, however, that Reactions 3 and 4 are almost independent of temperature. This observation suggests that net-transfer reactions involving dioctahedral exchange components in biotite can be applied to geologic barometry, provided that a model describing the chemical potentials of these components can be calibrated.

TABLE 6. Excess chemical potentials of dioctahedral exchange components

P kbar	T °C	ln K_3^*	ln K_3	$\mu^{ex}_{Mg\text{-}dic}$ kJ/mol	ln K_4^*	ln K_4	$\mu^{ex}_{Fe\text{-}dic}$ kJ/mol
			Including Fe^{3+} in biotite				
7	825	−5.618	−2.118	31.95	−2.599	1.222	34.88
7	850	−6.329	−2.049	39.96	−3.147	1.136	40.00
7	875	−5.906	−2.003	37.25	−2.975	1.032	38.24
7	900	−6.038	−1.957	39.80	−3.092	0.932	39.24
7	925	−6.107	−1.911	41.79	−2.899	0.836	37.21
7	950	−6.169	−1.842	44.00	−3.461	0.767	43.00
10	825	−5.146	−1.520	33.11	−2.366	1.899	38.93
10	850	−5.376	−1.497	36.22	−2.227	1.765	37.27
10	875	−5.215	−1.451	35.93	−2.381	1.659	38.56
10	900	−5.350	−1.405	38.48	−2.131	1.557	35.97
10	925	−5.079	−1.382	36.83	−2.244	1.437	36.66
10	950	−5.107	−1.335	38.35	−2.431	1.344	38.39
10	975	−5.576	−1.289	44.48	−1.858	1.254	32.30
13	900	−4.355	−0.967	33.04	−1.645	2.068	36.21
13	950	−4.562	−0.829	37.96	−1.746	1.920	37.28
			Assuming all Fe in biotite is Fe^{2+}				
7	825	−5.716	−2.118	32.84	−2.914	1.222	37.76
7	850	−6.347	−2.049	40.13	−3.165	1.136	40.16
7	875	−5.946	−2.003	37.63	−3.141	1.032	39.82
7	900	−6.114	−1.957	40.55	−3.384	0.932	42.09
7	925	−6.171	−1.911	42.43	−3.180	0.836	40.01
7	950	−6.189	−1.842	44.21	−3.734	0.767	45.77
10	825	−5.160	−1.520	33.23	−2.411	1.899	39.34
10	850	−5.393	−1.497	36.38	−2.273	1.765	37.70
10	875	−5.253	−1.451	36.29	−2.512	1.659	39.81
10	900	−5.395	−1.405	38.92	−2.297	1.557	37.59
10	925	−5.125	−1.382	37.29	−2.443	1.437	38.65
10	950	−5.136	−1.335	38.65	−2.582	1.344	39.92
10	975	−5.610	−1.289	44.83	−2.080	1.254	34.60
13	900	−4.388	−0.967	33.36	−1.835	2.068	38.06
13	950	−4.584	−0.829	38.18	−1.954	1.920	39.40

A working model for nonideal mixing of Mg-Fe-[6]Al-Ti in biotite

In order to determine values for cationic interpretation parameters from the observed excess chemical potentials, it is necessary to fit these excess chemical potentials to some function of biotite composition. In the strict sense, because exchange components are being used and these components are defined as differences between additive components, such a procedure will only yield differences between interaction parameters. A number of simplifying assumptions can be made, however, which can lead to reasonable estimates of the absolute values of some of these interaction parameters.

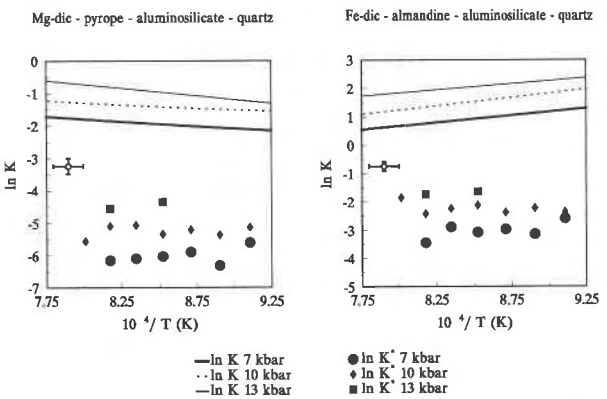

Fig. 5. Measured equilibrium positions for net-transfer Reactions 3 and 4 (K_3^*, Eq. 27, and K_4^*, Eq. 28), compared with calculated equilibrium positions for net-transfer Reactions 21 and 22 among pure end-member additive components (K_3 and K_4, curves, calculated with sillimanite at 7 and 10 kbar and kyanite at 13 kbar). Values of K^* calculated for biotite stoichiometries including Fe^{3+}. Representative uncertainties (shown by crosses) estimated by propagating uncertainties in biotite and garnet compositions (see text).

As a first approximation, we will assume that all nonideality in biotite is restricted to the two M2 octahedral sites. Ignoring tetrahedral nonideality at this stage is justified because tetrahedral contributions cancel out in the ideal activity-composition expressions that we derived for the dioctahedral exchange vectors. Neglecting the nonideal contribution of the [6]M1 site is a consequence of our assumption about octahedral ordering in biotite, namely that only Fe^{2+}, Mg, and vacancies mix in this site. Linear changes in unit-cell dimensions along the phlogopite-annite join have been interpreted as implying that Fe^{2+} and Mg mix almost ideally in binary biotite solid solution (e.g., Wones and Eugster, 1965; Mueller, 1972; Hewitt and Wones, 1975). Sack and Ghiorso (1989) have suggested, however, that binary Fe-Mg mixing in biotite is better described by a regular solution model with an interaction parameter (W_{FeMg}) on the order of 15–20 kJ/mol. Although this energetic contribution is not negligible, it is small compared with those arising from Mg-Fe-Al-Ti mixing (see below). More importantly, however,

the standard state thermodynamic properties of annite employed in this study (from Berman, 1990) rely heavily on the assumption that Fe-Mg mixing in biotite in the experiments of Ferry and Spear (1978) is ideal, so that including nonideal Fe-Mg mixing terms in our model does not appear warranted.

The only remaining nonideality is that derived from mixing Mg, Fe^{2+}, Al, Ti, and Fe^{3+} in the two M2 sites. Because of the uncertainties involved in estimating Fe^{3+} contents, this component will be considered in the calculation of mole fractions (cf. Table 5), but it will not be included in the mixing model. The excess free energy of mixing can then be approximated by means of a quaternary subregular model (e.g., Wohl, 1946; Thompson, 1967; Helffrich and Wood, 1989), which can be simplified considerably by assuming that the energetic contributions of ternary interactions are negligible compared with those of binary interactions. The latter assumption is valid in many minerals, but it is not necessarily always true (see Helffrich and Wood, 1989). We believe, however, that the density of our data set does not allow for the inclusion of ternary parameters in the model and that doing so would amount to overfitting the data. Moreover, application of the model to rocks (beyond the P-T-composition space covered by the experiments) shows that consideration of binary interactions alone is sufficient to generate reasonable estimates of the excess chemical potentials of the dioctahedral components. If we neglect ternary interactions, the quaternary subregular model (after Helffrich and Wood, 1989) results in the following expressions for activity coefficients calculated on a two-site basis (i.e., two M2 sites):

$$\begin{aligned} RT \ln \gamma_{Mg} = {} & (1 - X_{Mg})(W_{MgFe}X_{Fe} + W_{MgAl}X_{Al} + W_{MgTi}X_{Ti}) \\ & - X_{Fe}(W_{FeAl}X_{Al} + W_{FeTi}X_{Ti}) \\ & - X_{Al}X_{Ti}W_{AlTi} \end{aligned} \quad (29)$$

$$\begin{aligned} RT \ln \gamma_{Fe} = {} & (1 - X_{Fe})(W_{FeAl}X_{Al} + W_{FeTi}X_{Ti} + W_{FeMg}X_{Mg}) \\ & - X_{Al}(W_{AlTi}X_{Ti} + W_{AlMg}X_{Mg}) \\ & - X_{Ti}X_{Mg}W_{TiMg} \end{aligned} \quad (30)$$

$$\begin{aligned} RT \ln \gamma_{Al} = {} & (1 - X_{Al})(W_{AlTi}X_{Ti} + W_{AlMg}X_{Mg} + W_{AlFe}X_{Fe}) \\ & - X_{Ti}(W_{TiMg}X_{Mg} + W_{TiFe}X_{Fe}) \\ & - X_{Mg}X_{Fe}W_{MgFe}. \end{aligned} \quad (31)$$

Note that mole fractions in these equations are mole fractions in the M2 octahedral sites (as defined in Table 5), and that, because the activity coefficients are defined on a two-site basis and all nonideality is assumed to reside in these two sites, $\gamma_{mus} = \gamma_{Al}$, $\gamma_{phl} = \gamma_{Mg}$, and $\gamma_{ann} = \gamma_{Fe}$.

Two additional simplifying assumptions can be introduced. First, we will assume that nonideal interactions in biotite are symmetric, so that in every case $W_{ij} = W_{ji}$ (where i and j stand for Mg, Fe, Al, or Ti). Second, in keeping with the assumed ideality of Fe-Mg mixing, W_{MgFe} will be set equal to zero. The explicit formulations for the excess chemical potentials of Mg-dioctahedral and Fe-dioctahedral exchange components then simplify to

$$\begin{aligned} \mu^{ex}_{Mg\text{-}dic} &= RT \ln \gamma_{Mg\text{-}dic} = RT(\ln \gamma_{Al} - \ln \gamma_{Mg}) \\ &= (X_{Mg} - X_{Al})W_{MgAl} + X_{Fe}W_{FeAl} \\ &\quad + X_{Ti}(W_{AlTi} - W_{MgTi}) \end{aligned} \quad (32)$$

$$\begin{aligned} \mu^{ex}_{Fe\text{-}dic} &= RT \ln \gamma_{Fe\text{-}dic} = RT(\ln \gamma_{Al} - \ln \gamma_{Fe}) \\ &= (X_{Fe} - X_{Al})W_{FeAl} + X_{Mg}W_{MgAl} \\ &\quad + X_{Ti}(W_{AlTi} - W_{FeTi}). \end{aligned} \quad (33)$$

Examination of these equations shows that they contain four independent parameters: W_{MgAl}, W_{FeAl}, $W_{AlTi} - W_{MgTi}$ and $W_{AlTi} - W_{FeTi}$.

Linear programming analysis of excess chemical potentials in biotite

Linear programming makes it possible to optimize the value of an objective function while maintaining consistency with inequality constraints provided by experimental data (e.g., Gordon, 1973). This technique was used to fit the excess chemical potentials shown in Table 6 to the solution models described by Equations 32 and 33. Interaction parameters derived by linear programming will in general not be unique solutions, but they will be internally consistent and also consistent with the standard-state thermodynamic properties on which they are based. Because of these properties, the interaction parameters will be useful in geological thermometry and barometry. Moreover, given estimates of their probable uncertainties, these interaction parameters will provide good starting points for further refinement.

In order to carry out a linear programming optimization, it is necessary to set up a system of linear inequalities that constrain the model. This was accomplished by making use of the pressure and temperature uncertainties of each experiment. Experiments were spaced 25 °C apart (cf. Table 1), and both mineral and melt compositions and modes (see also Patiño Douce and Johnston, 1991) change in smooth and regular ways between consecutive experiments. This behavior suggests that the temperature uncertainty cannot be much larger than half the temperature spacing between consecutive experiments, so we have adopted a value of ±15 °C for this uncertainty (shown in Figs. 2, 4, 5). Uncertainty in pressure is estimated at ±500 bars. Pressure during the experiments was kept within 100 bars of the target pressure. Because friction corrections in NaCl cell assemblies are small (e.g., Bohlen, 1984), an uncertainty of ±500 bars appears to be quite conservative.

These uncertainties in temperature and pressure were used to generate a system of linear inequalities in the following manner. Let the Gibbs free energy change for the Mg end-member additive component reaction (Reaction 21) at the nominal P and $T(P_N,T_N)$ of the experi-

TABLE 7. Excess mixing parameters estimated by linear programming

	W_{MgAl}	W_{FeAl}	$W_{AlTi} - W_{MgTi}$	$W_{AlTi} - W_{FeTi}$
Model 1. Including Fe^{3+} in biotite				
Preferred value (kJ/mol)	52.2	74.4	47.8	60.1
Probable uncertainty (kJ/mol)	−10.0	+10.0	−15.0	+15.0
Number of inequalities in data set: 50				
Model 2. Assuming all Fe in biotite is Fe^{2+}				
Preferred value (kJ/mol)	54.7	57.4	65.1	75.1
Probable uncertainty (kJ/mol)	+3.0	+6.0	−6.0	−15.0
Number of inequalities in data set: 44				

Note: Excess parameters for Mg-Fe^{2+}-Al-Ti mixing on two M2 sites. Values are for mole of biotite calculated on a 12-anion basis. Probable uncertainties estimated by optimizing a set of inequalities broadened by the uncertainties in the ideal activities of dioctahedral components in biotite and almandine and pyrope components in garnet (see text). Internally consistent data sets for these broader inequalities contained 56 data points for both models.

ment be ΔG^0_N. If ΔP, ΔT are the pressure and temperature uncertainties, then for this particular end-member reaction within the pressure-temperature range of the experiments the following relationships hold:

$$0 < \Delta G^0_A < \Delta G^0_N < \Delta G^0_B \tag{34}$$

for

$$P_A = P_N + \Delta P, \qquad T_A = T_N + \Delta T$$
$$P_B = P_N - \Delta P, \qquad T_B = T_N - \Delta T. \tag{35}$$

If the experimental product represents an equilibrium assemblage at some unknown pressure, P, and temperature, T, within this interval, then

$$0 < \Delta G^0_A \le \Delta G^0_{P,T} = -RT \ln K_3 \le \Delta G^0_B \tag{36}$$

where $\Delta G^0_{P,T}$ is the Gibbs free energy change of Reaction 21 between pure end-member components at P and T. Because

$$\ln K_3 = \ln K_3^* + \ln \gamma_{Mg\text{-}dic} \tag{37}$$

(see Eqs. 23 and 27), Equation 36 can be rearranged as follows:

$$-\Delta G^0_B - RT \ln K_3^* \le RT \ln \gamma_{Mg\text{-}dic} \le -\Delta G^0_A - RT \ln K_3^* \tag{38}$$

From this relationship, and noting (see Table 6) that

$$\ln K_3^* < 0 \tag{39}$$

and that (see Eq. 35)

$$T_B \le T \le T_A \tag{40}$$

the following inequality is derived:

$$-G^0_B - RT_B \ln K_3^* \le RT \ln \gamma_{Mg\text{-}dic} \le -\Delta G^0_A - RT_A \ln K_3^*. \tag{41}$$

Equation 41 provides two inequality constraints for the excess chemical potential of the Mg-dioctahedral exchange component in each experiment. A similar analysis leads to another two inequality constraints for the Fe-dioctahedral exchange component, except that the Gibbs free energy changes and temperature and pressure intervals must in this case be chosen as follows:

$$\Delta G^0_A < \Delta G^0_N < \Delta G^0_B < 0 \tag{42}$$

for

$$P_A = P_N + \Delta P, \qquad T_A = T_N - \Delta T$$
$$P_B = P_N - \Delta P, \qquad T_B = T_N + \Delta T. \tag{43}$$

The set of four inequalities for each experiment were used in conjunction with Equations 32 and 33 to define a feasible solution space for the four parameters: W_{MgAl}, W_{FeAl}, $W_{AlTi} - W_{MgTi}$ and $W_{AlTi} - W_{FeTi}$. The values of W_{MgAl} and W_{FeAl} were constrained to be larger than zero, whereas the differences $W_{AlTi} - W_{MgTi}$ and $W_{AlTi} - W_{FeTi}$ were constrained to the interval −500 to 500 kJ/mol. In order to choose the optimum solution within the feasible solution space, it is necessary to define an objective function whose value can be either minimized or maximized. The study of Williams and Grambling (1990) of natural Al-rich biotite concluded that the difference between the magnitudes of Mg-Al and Fe-Al excess free energies of mixing is small or negligible. This conclusion, which is qualitatively consistent with the purported near-ideality of Fe-Mg mixing, suggests minimization of the following objective function, F:

$$F = |W_{MgAl} - W_{FeAl}|. \tag{44}$$

The values of the excess mixing parameters presented in Table 7 were estimated by minimizing the value of F within the feasible solution space defined by the inequality constraints (Eq. 41 and the equivalent relationship for $\gamma_{Fe\text{-}dic}$). In order to test the robustness of this solution, we carried out parallel optimizations in which F was defined in alternative ways: minimizing the difference $|W_{MgTi} - W_{FeTi}|$, or the sum $|W_{MgAl} - W_{FeAl}| + |W_{MgTi} - W_{FeTi}|$. In every case we obtained mixing parameters that were within 0.1–5 kJ/mol of those shown in Table 7. These results create confidence in the estimated parameters because their values are not very sensitive to the particular choice of objective function.

Linear programming was performed by adding one datum (i.e., one pair of inequalities constraining either Reaction, 3 or 4) at a time, so as to group data points in various internally consistent sets. This routine was performed iteratively with the goal of finding the largest possible internally consistent data set. Of the 15 experiments used for this study, only one (the experiment at 975 °C, 10 kbar, see Figs. 3–5) was always found to be inconsistent with all the other experiments. This suggests that either the small amount of biotite (about 2%, Patiño Douce and Johnston, 1991) present in this charge persisted metastably or that some of the assumptions made in calculating its stoichiometry are no longer valid at these conditions. In particular, the anhydrous weight total for

this composition is very close to 100%, indicating that biotite in this experiment may be essentially anhydrous.

Two sets of interaction parameters were obtained (Models 1 and 2, Table 7), calculated with different assumptions about Fe^{3+} in biotite. Model 1 was derived using Fe^{3+} values in biotite from Table 3, whereas Model 2 assumes no Fe^{3+} in biotite. Discarding the always inconsistent data described in the preceding paragraph leaves a maximum possible total of 56 inequality constraints, of which the largest internally consistent data sets contain 50 and 44 inequalities for Models 1 and 2, respectively (see Table 7). These numbers indicate that the feasible solution spaces for both models are substantially overdetermined, and therefore provide additional support in favor of a reasonable approach to equilibrium during the experiments. In both models the same garnet formulae (which include Fe^{3+}, cf. Table 2) were used. Of course, assuming that biotite in equilibrium with Fe^{3+}-bearing garnet is itself free of Fe^{3+} (i.e., Model 2) is not strictly justified, and this may be the reason why Model 2 is associated with a smaller internally consistent data set than Model 1. In any event, comparison between both sets of interaction parameters and comparison of P-T estimates for the same natural assemblages obtained with Models 1 and 2 (next section) will provide insight about the effect that Fe^{3+} content in biotite has on the calculated positions of biotite-bearing equilibria.

Uncertainties in the values of the interaction parameters were estimated as follows. The errors of the mean biotite compositions (2 sd, cf. Table 3) were propagated to obtain the uncertainties in the ideal activities of the Mg-dioctahedral and Fe-dioctahedral exchange components (shown in Fig. 4). Uncertainties in the ideal activities of garnet components were taken to be those arising from counting statistics alone because garnet compositions are taken from single analyses. Uncertainties in the excess chemical potentials of the dioctahedral exchange components, arising from the uncertainties in the ideal activities of biotite and garnet, were characteristically found to be about 1.5–2 kJ/mol. The uncertainties in the ideal activities were also used to broaden the inequality constraints, and the new system of inequalities was optimized by minimizing the objective function, F (Eq. 44). It was found that this led to internally consistent data sets that included all data points in both models, except the experiment at 975 °C and 10 kbar. The interaction parameters varied, relative to the values calculated initially, by 3–15 kJ/mol (see Table 7). Note that with this procedure it is not possible to obtain an uncertainty interval around the preferred value. Rather, the results in Table 7 suggest, for example, that W_{MgAl} is likely to be within the interval 42.2–52.2 kJ/mol (for Model 1) or 54.7–57.7 kJ/mol (for Model 2).

Applications to thermometry and barometry of natural assemblages

The biotite solution model was tested by utilizing it to estimate internally consistent pressures and temperatures of crystallization of mineral assemblages reported in the literature. The chosen assemblages are such that they allow calculation of both pressure and temperature from equilibria involving the dioctahedral exchange components in biotite (and their linear combination, $FeMg_{-1}$). For example, the assemblage garnet + biotite + aluminosilicate + quartz permits calculation of pressure from Reaction 3 (see Fig. 5) and temperature from garnet-biotite Fe-Mg exchange. From the assemblage cordierite + biotite + aluminosilicate + quartz, it is possible to calculate temperature from biotite-cordierite Fe-Mg exchange and pressure from the net-transfer reaction

$$8Al_2SiO_5 + 7SiO_2 \leftrightarrow 2(Al_2Mg_{-3})_{bio} + 3(Mg_2Al_4Si_5O_{18})_{crd}. \quad (45)$$

Finally, in the aluminosilicate-absent assemblage garnet + cordierite + biotite + quartz, temperature can be estimated from any of three Fe-Mg exchange equilibria and pressure from

$$3(Mg_2Al_4Si_5O_{18})_{crd} \leftrightarrow 2(Al_2Mg_{-3})_{bio} + 4(Mg_3Al_2Si_3O_{12})_{gar} + 3SiO_2. \quad (46)$$

The combination of Equations 32 and 33 yields the excess chemical potential of the $FeMg_{-1}$ exchange component in biotite, as follows:

$$\begin{aligned} RT \ln \gamma_{FeMg_{-1}} &= RT(\ln \gamma_{Fe} - \ln \gamma_{Mg}) \\ &= X_{Al}(W_{FeAl} - W_{MgAl}) \\ &\quad + X_{Ti}(W_{FeTi} - W_{MgTi}) \end{aligned} \quad (47)$$

with

$$W_{FeTi} - W_{MgTi} = (W_{AlTi} - W_{MgTi}) - (W_{AlTi} - W_{FeTi}). \quad (48)$$

Pressures determined from any of these equilibria rely on dioctahedral exchange components in biotite, and such methodology has not (to our knowledge) been rigorously applied before. In this sense, the solution model that we propose does not represent a refinement of models already being used, but rather an altogether new way of using biotite in the estimation of intensive variables. If the calculated pressures are consistent with independent pressure constraints, it would signify that the Mg-dioctahedral and Fe-dioctahedral exchange components can be applied to thermobarometry of metamorphic and igneous rocks in which few other useful equilibria occur. Most importantly, because nonideality of the dioctahedral exchange components is quite large (cf. Fig. 5, Table 6), the fact that reasonable pressure values are obtained is a good indication that the solution model proposed here yields acceptable approximations to the chemical potentials of these components.

Internally consistent pressures and temperatures were solved simultaneously, by iterating between the corresponding exchange and net-transfer equilibria until consecutive values of P and T were within specified conver-

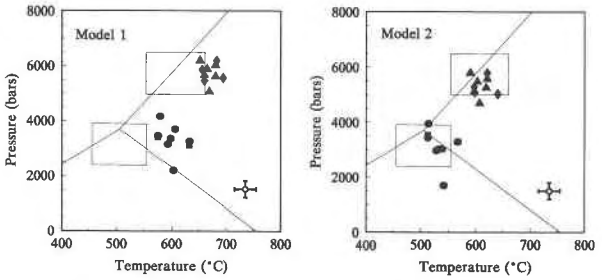

● Hodges & Spear (1982), sil-bearing
■ Hodges & Spear (1982), and-bearing
♦ Pigage (1982), sil-bearing
▲ Pigage (1982), sil- & ky-bearing

Fig. 6. Internally consistent P-T conditions (symbols, estimated from Mg-dioctahedral + garnet + aluminosilicate + quartz net-transfer equilibrium and exchange of Fe and Mg between garnet and biotite) for sillimanite- and andalusite-bearing assemblages from Hodges and Spear (1982) and sillimanite-bearing assemblages (±kyanite) from Pigage (1982). Estimated uncertainties (see text) shown by crosses. Rectangles show ranges in P-T conditions estimated by Hodges and Spear (lower) and Pigage (upper).

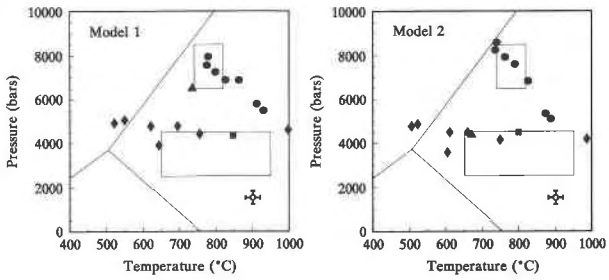

▲ Grant & Frost (1990), sil- & gar-bearing
■ Grant & Frost (1990), sil- & crd-bearing
♦ Grant & Frost (1990), gar- & crd-bearing
● Indares & Martignole (1984, 1985)

Fig. 7. Internally consistent P-T conditions (symbols, estimated from Mg-dioctahedral + garnet + aluminosilicate + quartz, Mg-dioctahedral + cordierite + aluminosilicate + quartz and Mg-dioctahedral + garnet + cordierite + quartz net-transfer equilibria and garnet-biotite or cordierite-biotite Fe-Mg exchange equilibria) for assemblages from Grant and Frost (1990) and for sillimanite-bearing metapelitic assemblages from the Maniwaki area (Indares and Martignole, 1984). Estimated uncertainties (see text) shown by crosses. Rectangles show ranges in P-T conditions estimated by Grant and Frost (lower) and Indares and Martignole (upper), in both cases constrained by biotite-independent equilibria.

gence intervals (50 bars and 5 °C). All standard-state thermodynamic properties and heat-capacity coefficients were taken from Berman (1988, 1990). Compressibilities and coefficients of thermal expansion were ignored because their contributions to the Gibbs free energy change of reaction are small compared with the uncertainties in the biotite interaction parameters. A combined Newton-Raphson bisection root-finding algorithm (Press et al., 1989, p. 258) was used to solve the nonlinear equations that result from including the heat-capacity terms in the expression for the Gibbs free energy change of reaction. Mixing in garnet was modeled after Berman (1990), whereas cordierite was assumed to be anhydrous, and Fe-Mg mixing in it was considered ideal. Only assemblages containing sillimanite or andalusite were included in the analysis of aluminosilicate-bearing equilibria. Assemblages containing kyanite as the only aluminosilicate polymorph are not suitable because Reactions 21 and 22 with kyanite have relatively small volume changes and large entropy changes, so that their Clapeyron slopes are too steep to serve as practical barometers.

Figure 6 shows the results obtained from amphibolite-grade garnet + biotite + aluminosilicate + quartz assemblages reported by Hodges and Spear (1982) and Pigage (1982). Although temperature estimates presented by these authors are not independent of biotite equilibria, these studies are particularly useful because P-T conditions in both cases are constrained by aluminosilicate phase relationships. Hodges and Spear (1982) estimated pressures from the garnet + plagioclase + aluminosilicate + quartz equilibrium and proposed conditions (also suggested by field evidence) in the neighborhood of the aluminosilicate triple point (lower rectangle in Fig. 6). These conditions are satisfactorily reproduced by Model 2 (which ignores Fe^{3+} in biotite in the experimental products). The rocks studied by Pigage (1982) traverse the sillimanite-kyanite phase boundary at a temperature (estimated on the basis of several equilibria in pelites and calc-silicates) of 605 ± 50 °C (upper rectangle in Fig. 6). Model 2 correctly places the P-T conditions very close to the kyanite-sillimanite phase boundary within this temperature range. In both of these examples, Model 1 (which accounts for Fe^{3+} in the experimental products) yields temperatures that are 50 to 100 °C too high (or pressures about 1 kbar too low) to be consistent with aluminosilicate phase relationships.

Examples of the application of the biotite solution model to granulite-facies rocks are shown in Figure 7. Maximum metamorphic temperatures in the Maniwaki area of the Grenville Province in Canada (Indares and Martignole, 1984), calculated with clinopyroxene-garnet Fe-Mg exchange, range from 740 to 820 °C, whereas maximum pressures are in the range 6.5–8.5 kbar, calculated from pyroxene + plagioclase + garnet + quartz and plagioclase + garnet + sillimanite + quartz equilibria. Application of the Ferry and Spear (1978) garnet-biotite geothermometer to these rocks, however, produces temperatures in the range 900–1065 °C, and this discrepancy led Indares and Martignole (1985) to develop an empirical calibration for garnet-biotite Fe-Mg exchange based on samples from the Maniwaki area. Figure 7 shows internally consistent pressures and temperatures calculated from garnet + biotite + aluminosilicate + quartz assemblages from the Maniwaki metapelites (data from Indares and Martignole, 1984, and Martignole, personal communication). With the exception of two samples, both Models 1 and 2 satisfactorily reproduce the metamorphic

P-T conditions estimated by Indares and Martignole (1984, upper rectangle in Fig. 7). This result is particularly important because it does not rely on any other biotite solution model to test the merits of the mixing model proposed here.

The lower rectangle in Figure 7 shows the range in *P-T* conditions for the contact aureole of the Laramie anorthosite complex (Grant and Frost, 1990), also estimated in part on the basis of biotite-absent equilibria. Pressures calculated from different samples and with each of the three biotite-bearing net-transfer equilibria (Equilibria 3, 45, and 46) are remarkably constant (especially for Model 2), whereas temperatures span a relatively wide interval. Such a pattern is consistent with a contact-metamorphic recrystallization episode. Results from Model 2 are in reasonable agreement with the conditions estimated by Grant and Frost (1990), except for some samples that yield temperatures that are lower than these authors' estimates. This could be a consequence of continued operation (in some rocks) of both exchange and net-transfer equilibria affecting biotite, during near-isobaric cooling of the contact aureole. Thus, pressure-temperature estimates obtained from biotite-bearing equilibria are not necessarily inconsistent with the constraints provided by Grant and Frost (1990) but, rather, reflect different closing temperatures (at constant pressure) for different rocks.

These four examples suggest that the biotite solution model that we propose can satisfactorily predict the chemical potentials of the exchange components Al_2Mg_{-3} and Al_2Fe_{-3} (and hence of their linear combination, $FeMg_{-1}$), at least within aluminous assemblages in which biotite composition is similar to that in the experimental products (Table 3). Simultaneous analysis of exchange and net-transfer reactions, which mediate equilibrium of these biotite exchange components with garnet, cordierite, aluminosilicate, and quartz, are capable of yielding reasonable, internally consistent pressures and temperatures over a wide range of amphibolite- and granulite-grade conditions. In the examples investigated, these estimates agree with independent *P-T* constraints, although agreement appears to be better using Model 2, in which Fe^{3+} in the experimental biotite is ignored. This does not necessarily imply that Fe^{3+} is not present in our experimental products. Rather, closer agreement with Model 2 might be a consequence of the fact that Fe^{3+} has also been ignored in the four studies discussed above. Note that in the two cases in which results from Models 1 and 2 diverge most (Fig. 6) temperatures calculated with Model 1 are too high. If Fe^{3+} were included in the biotite analyses of Hodges and Spear (1982) and Pigage (1982), then estimated temperatures would decrease. Results from Model 1 could then agree better with aluminosilicate phase relationships than results from Model 2.

This hypothesis can be tested by using data from Williams and Grambling (1990), who have determined (either directly or indirectly) Fe^{3+} contents in biotite from medium-grade metamorphic rocks from New Mexico. Peak metamorphic conditions in the Truchas Range appear to have been close to the aluminosilicate triple point and are shown (after Grambling et al., 1989) by the rectangles in Figure 8. Pressure-temperature conditions estimated with our model and with biotite compositions from Williams and Grambling (1990), which include Fe^{3+}, are also shown in Figure 8 (circles). In this case net-transfer Reaction 3 and garnet-biotite Fe-Mg exchange yield results more consistent with aluminosilicate triple-point conditions if Model 1 is used to account for nonideality in biotite. Model 2, which ignores Fe^{3+} in biotite in our experimental products, yields temperatures that are too low (compare Fig. 6). We have also recalculated Williams and Grambling's (1990) biotite compositions assuming that all Fe is Fe^{2+} and used these compositions to estimate *P-T* conditions (Fig. 8, squares). Conditions calculated from Model 2 are now close to the aluminosilicate triple point, whereas Model 1 appears to overestimate temperature (compare Fig. 6). These results suggest that estimated Fe^{3+} contents in the experimental products are probably reasonable and that Model 1 is a better representation of the excess mixing properties of biotite than Model 2. However, unless Fe^{3+} is also determined in the biotite to which the model is applied, Model 2 is likely to generate better *P-T* estimates than Model 1.

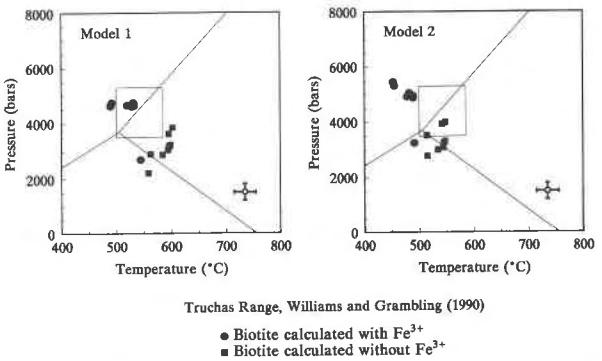

Fig. 8. Internally consistent *P-T* conditions (symbols, estimated from Mg-dioctahedral + garnet + aluminosilicate + quartz net-transfer equilibrium and exchange of Fe and Mg between garnet and biotite) for sillimanite- and andalusite-bearing assemblages from the Truchas Range. Circles show results using Fe^{3+} estimates from Williams and Grambling (1990), squares show results assuming that all Fe in biotite is Fe^{2+}. Estimated uncertainties (see text) shown by crosses. Rectangles show range in *P-T* conditions estimated by Grambling et al. (1989).

The effect of the likely uncertainties in the interaction parameters (cf. Table 7) on the pressure-temperature determinations was also investigated. In order to do so, we calculated a new set of *P-T* values using interaction parameters as removed from the values in Table 7 as their uncertainties would allow. The new pressures were within 500 and 350 bars (for Models 1 and 2, respectively) of the pressures calculated initially, whereas temperatures were within 35 °C of the initial values for both models. For Model 2 new pressures and temperatures were consistently higher than those calculated initially, whereas no

such clear trend was observed for Model 1. The uncertainties in pressure and temperature estimates derived from dioctahedral exchange components are comparable to those associated with other mineral equilibria.

Discussion and conclusions

Although the results obtained from applying the biotite solution model to natural assemblages are encouraging, it must be stressed that this is a working model, which is far from providing a complete thermodynamic description of biotite. Among its most obvious shortcomings are the facts that the model was calibrated from a single bulk composition and over a restricted pressure-temperature range. Attempts were made to determine the temperature and pressure dependencies of the interaction parameters (i.e., values for W_s and W_v) from the experimental data. We concluded, however, that the relatively small number of experiments, together with the restricted P-T range covered by them, did not permit a meaningful analysis.

Another problem that cannot be addressed in an entirely satisfactory manner arises from the unknown Fe^{3+} content in the experimental products used to calibrate the model. Table 7 shows that, whereas this uncertainty is not likely to affect the calculated value of W_{MgAl} in a significant way, estimates of W_{FeAl}, $W_{AlTi} - W_{MgTi}$ and $W_{AlTi} - W_{FeTi}$ are quite sensitive to the assumed Fe^{3+}-Fe^{2+} distribution in biotite. Sensitivity of the Fe-bearing parameters is easy to understand. The estimates of $W_{AlTi} - W_{MgTi}$ are affected because W_{MgTi} and W_{FeTi} are implicitly correlated when net-transfer Reactions 3 and 4 are solved simultaneously. Regardless of the Fe^{3+} content of biotite, however, the large positive values obtained for the differences $W_{AlTi} - W_{MgTi}$ and $W_{AlTi} - W_{FeTi}$ indicate that the excess free energy arising from Al-Ti mixing in biotite is considerably greater than Mg-Ti and Fe-Ti excess free energies of mixing. This result is consistent with the Al-Ti avoidance observed in biotite from natural metapelitic assemblages containing Ti-saturating phases (cf. Guidotti, 1984).

Yet another aspect of mixing in biotite that needs additional work is that of cationic ordering and its effect on activity-composition relationships. The purely macroscopic model developed here relies on what appear to be reasonable assumptions about cationic ordering in micas. It would be preferable, however, to develop a mixing model that incorporates microscopic aspects of biotite mixing and in which activities are functions of both compositional and ordering variables (cf. Ghiorso, 1990). We suggest that future experimental work should be designed so as to provide the required data base for such an approach.

Our results demonstrate the feasibility of using net-transfer reactions involving Mg-dioctahedral and Fe-dioctahedral exchange components of biotite in barometry of assemblages that buffer the chemical potential of Al (e.g., containing at least a pair of the following phases: garnet, aluminosilicate, cordierite, staurolite, aluminate spinel, corundum). This should find important applications in medium- and high-grade metapelitic rocks, by providing pressure estimates independent of commonly used equilibria that involve anorthite and grossular. The use of dioctahedral components in biotite could be particularly important in relatively low-pressure rocks, in which the grossular content of garnet is small (5 mol% or less), and hence its activity coefficient very poorly constrained.

Acknowledgments

We thank M. Kohn, M.J. Holdaway, B. Mukhopadhyay, and R. Berman for reviewing an earlier version of this manuscript and offering valuable and helpful comments, and we thank M. Kohn and D. Hewitt for offering very helpful criticism of the last version of the manuscript. Discussions with Carolyn Rebbert helped A.E.P.D. to better understand mixing of trioctahedral and dioctahedral micas. We also thank J. Martignole for making available unpublished mineral analyses that were necessary to test our model with the Maniwaki rocks and J. Grambling for providing detailed information about mineral assemblages of the rocks from New Mexico. The experiments used for this work were done while the senior author was a graduate student at the University of Oregon supported by NSF grants EAR-8720150 and EAR-8915624 to Johnston. Most of the probe analyses were done at the University of Oregon, where the probe facility was funded by NSF grant EAR-8803960 and a matching grant from the Keck Foundation. Additional analyses were done at the University of Georgia, where the probe facility was funded by NSF grant EAR-8816748 and a matching grant from the University of Georgia Research Foundation.

References cited

Abrecht, J.A., and Hewitt, D.A. (1988) Experimental evidence on the substitution of Ti in biotite. American Mineralogist, 73, 1275–1284.

Bailey, S.W. (1984) Crystal chemistry of the true micas. In Mineralogical Society of America Reviews in Mineralogy, 13, 13–60.

Barbey, P., Macaudiere, J., and Nzenti, J.P. (1990) High-pressure dehydration melting of metapelites: Evidence from the migmatites of Yaoundé (Cameroon). Journal of Petrology, 31, 401–427.

Berman, R.G. (1988) Internally-consistent thermodynamic data for stoichiometric minerals in the system Na_2O-K_2O-CaO-MgO-FeO-Fe_2O_3-Al_2O_3-SiO_2-TiO_2-H_2O-CO_2. Journal of Petrology, 29, 445–522.

——— (1990) Mixing properties of Ca-Mg-Fe-Mn garnets. American Mineralogist, 75, 328–344.

Bohlen, S.R. (1984) Equilibria for precise pressure calibration and a frictionless furnace assembly for the piston-cylinder apparatus. Neues Jahrbuch für Mineralogie Monatshefte, 9, 404–412.

Bohlen, S.R., and Essene, E.J. (1980) Evaluation of coexisting garnet-biotite, garnet-clinopyroxene and other Mg-Fe exchange thermometers in Adirondack granulites. Geological Society of America Bulletin, 91, 685–719.

Brigatti, M.F., Galli, E., and Poppi, L. (1991) Effect of Ti substitution in biotite-*1M* crystal chemistry. American Mineralogist, 76, 1174–1183.

Burnham, C.W. (1979) The importance of volatile constituents. In H.S. Yoder, Ed., The Evolution of the igneous rocks, p. 439–482. Princeton University Press, Princeton, New Jersey.

Carroll, M.R., and Wyllie, P.J. (1990) The system tonalite-H_2O at 15 kbar and the genesis of calc-alkaline magmas. American Mineralogist, 75, 345–357.

Chipera, S.J., and Perkins, D. (1988) Evaluation of biotite-garnet geothermometers: Application to the English River subprovince, Ontario. Contributions to Mineralogy and Petrology, 98, 40–48.

Circone, S., Navrotsky, A., Kirkpatrick, R.J., and Graham, C.M. (1991) Substitution of $^{[6,4]}$Al in phlogopite: Mica characterization, unit-cell variation, ^{27}Al and ^{29}Si MAS-NMR spectroscopy, and Al-Si distribution in the tetrahedral sheet. American Mineralogist, 76, 1485–1501.

Dymek, R.F. (1983) Titanium, aluminum, and interlayer cation substitutions in biotite from high-grade gneisses, West Greenland. American Mineralogist, 68, 880–899.

Edwards, R.L., and Essene, E.J. (1987) Pressure, temperature and C-O-H fluid fugacities across the amphibolite-granulite transition, northwest Adirondack Mountains, New York. Journal of Petrology, 29, 39–72.

Essene, E.J. (1989) The current status of thermobarometry in metamorphic rocks. Geological Society Special Publication, 43, 1–44.

Ferry, J.M., and Spear, F.S. (1978) Experimental calibration of the partitioning of Fe and Mg between biotite and garnet. Contributions to Mineralogy and Petrology, 66, 113–117.

Ghiorso, M.S. (1990) Application of the Darken equation to mineral solid solutions with variable degrees of order-disorder. American Mineralogist, 75, 539–543.

Gordon, T.M. (1973) Determination of internally consistent thermodynamic data from phase equilibrium experiments. Journal of Geology, 81, 199–208.

Grambling, J.A., Williams, M.L., Smith, R.F., and Mawer, C.K. (1989) The role of crustal extension in the metamorphism of Proterozoic rocks in northern New Mexico. Geological Society of America Special Paper, 235, 87–110.

Grant, J.A., and Frost, B.R. (1990) Contact metamorphism and partial melting of pelitic rocks in the aureole of the Laramie anorthosite complex, Morton Pass, Wyoming. American Journal of Science, 290, 425–472.

Guidotti, C.V. (1984) Micas in metamorphic rocks. In Mineralogical Society of America Reviews in Mineralogy, 13, 357–468.

Helffrich, G., and Wood, B. (1989) Subregular model for multicomponent solutions. American Mineralogist, 74, 1016–1022.

Hewitt, D.A., and Abrecht, J. (1986) Limitations on the interpretation of biotite substitutions from chemical analyses of natural samples. American Mineralogist, 71, 1126–1128.

Hewitt, D.A., and Wones, D.R. (1975) Physical properties of some synthetic Fe-Mg-Al trioctahedral biotites. American Mineralogist, 60, 854–862.

——— (1984) Experimental phase relations of the micas. In Mineralogical Society of America Reviews in Mineralogy, 13, 201–256.

Hodges, K.V., and Spear, F.S. (1982) Geothermometry, geobarometry and the Al_2SiO_5 triple point at Mt. Moosilauke, New Hampshire. American Mineralogist, 67, 1118–1134.

Hoisch, T.D. (1989) A muscovite-biotite geothermometer. American Mineralogist, 74, 565–572.

——— (1991) Equilibria within the mineral assemblage quartz + muscovite + biotite + garnet + plagioclase, and implications for the mixing properties of octahedrally-coordinated cations in muscovite and biotite. Contributions to Mineralogy and Petrology, 108, 43–54.

Holdaway, M.J. (1980) Chemical formulae and activity models for biotite, muscovite, and chlorite applicable to pelitic metamorphic rocks. American Mineralogist, 65, 711–719.

Holdaway, M.J., Dutrow, B.L., and Hinton, R.W. (1988) Devonian and Carboniferous metamorphism in west-central Maine: The muscovite-almandine geobarometer and the staurolite problem revisited. American Mineralogist, 73, 20–47.

Holland, T.J.B., and Powell, R. (1990) An enlarged and updated internally consistent thermodynamic dataset with uncertainties and correlations: The system K_2O-Na_2O-CaO-MgO-MnO-FeO-Fe_2O_3-Al_2O_3-TiO_2-SiO_2-C-H_2-O_2. Journal of Metamorphic Geology, 8, 89–124.

Indares, A., and Martignole, J. (1984) Evolution of *P-T* conditions during a high-grade metamorphic event in the Maniwaki area (Grenville Province). Canadian Journal of Earth Science, 21, 853–863.

——— (1985) Biotite-garnet geothermometry in the granulite facies: The influence of Ti and Al in biotite. American Mineralogist, 70, 272–278.

Kerrick, D.M., and Darken, L.S. (1975) Statistical thermodynamic models for ideal oxide and silicate solid solutions, with application to plagioclase. Geochimica et Cosmochimica Acta, 39, 1431–1442.

Labotka, T.C. (1983) Analysis of the compositional variations of biotite in pelitic hornfelses from northeastern Minnesota. American Mineralogist, 68, 900–914.

Mueller, R.F. (1972) Stability of biotite: A discussion. American Mineralogist, 57, 300–316.

Partin, E. (1984) Ferric/ferrous determination in synthetic biotite, 98 p. M.S. thesis, Virginia Polytechnic Institute and State University, Blacksburg, Virginia.

Patiño Douce, A.E., and Johnston, A.D. (1991) Phase equilibria and melt productivity in the pelitic system: Implications for the origin of peraluminous granitoids and aluminous granulites. Contributions to Mineralogy and Petrology, 107, 202–218.

Pigage, L.C. (1982) Linear regression analysis of sillimanite-forming reactions at Azure Lake, British Columbia. Canadian Mineralogist, 20, 349–378.

Press, W.H., Flannery, B.P., Teukolsky, S.A., and Vetterling, W.T. (1989) Numerical recipes in FORTRAN: The art of scientific computing, 702 p. Cambridge University Press, Cambridge, U.K.

Rebbert, C.R. (1986) Biotite oxidation: An experimental and thermodynamic approach, 70 p. M.S. thesis, Virginia Polytechnic Institute and State University, Blacksburg, Virginia.

Robert, J.L. (1976) Phlogopite solid solutions in the system K_2O-MgO-Al_2O_3-SiO_2-H_2O. Chemical Geology, 17, 195–212.

Ruendal, A.P. (1987) Petrology of sillimanite-grade metapelites in the Headquarters area, northern Idaho, 111 p. M.S. thesis, University of Oregon, Eugene, Oregon.

Sack, R.O., and Ghiorso, M.S. (1989) Importance of considerations of mixing properties in establishing an internally consistent thermodynamic database: Thermochemistry of minerals in the system Mg_2SiO_4-Fe_2SiO_4-SiO_2. Contributions to Mineralogy and Petrology, 102, 41–68.

Sen Gupta, P., Karmakar, S., Dasgupta, S., and Fukuoka, M. (1991) Petrology of spinel granulites from Araku, Eastern Ghats, India, and a petrogenetic grid for sapphirine-free rocks in the system FMAS. Journal of Metamorphic Geology, 9, 451–459.

Thompson, J.B. (1967) Thermodynamic properties of simple solutions. In P. Abelson, Ed., Researches in geochemistry, p. 340–361. Wiley, New York.

Williams, M.L., and Grambling, J.A. (1990) Manganese, ferric iron, and the equilibrium between garnet and biotite. American Mineralogist, 75, 886–908.

Wohl, K. (1946) Thermodynamic evaluation of binary and ternary liquid systems. Transactions of the American Institute of Chemical Engineering, 42, 215–249.

Wones, D.R., and Eugster, H.P. (1965) Stability of biotite: Experiment, theory and application. American Mineralogist, 50, 1228–1272.

Manuscript received January 10, 1992
Manuscript accepted September 16, 1992

Appendix 1: List of abbreviations used in the text

Als	aluminosilicate
Ann	annite
Bio	biotite
Crd	cordierite
Eas	eastonite
Fe-dic	Fe^{2+}-dioctahedral exchange component
Gar	garnet
Ilm	ilmenite
Mg-dic	Mg-dioctahedral exchange component
Mg-Tk	Mg-Tschermak's exchange component
Mus	muscovite
Phl	phlogopite
Qtz	quartz
Rut	rutile
a_i^{id}	ideal activity of component i
$a_i^{id,M}$	contribution of site M to the ideal activity of component i
γ_i	activity coefficient of component i
μ_i	chemical potential of component i
μ_i^0	standard-state chemical potential of component i
μ_i^{ex}	excess chemical potential of component i
ΔG_A^0	standard-state Gibbs free energy change of reaction at P-T conditions labeled A